Università Politecnica delle Marche
Scuola di Dottorato di Ricerca in Scienze dell'Ingegneria
Curriculum in Ingegneria Civile, Ambientale, Edile e Architettura
----

Facing the biodeterioration of construction and cultural heritage materials: a novel approach to predict algae growth on fired brick surfaces

Ph.D. Dissertation of:

Benedetta Gregorini

Advisor:

Prof. Marco D'Orazio

Coadvisor:

Prof. Enrico Quagliarini

Curriculum supervisor:

Prof. Francesco Fatone

XIX edition - new series

2

Università Politecnica delle Marche
Scuola di Dottorato di Ricerca in Scienze dell'Ingegneria
Curriculum in Ingegneria Civile, Ambientale, Edile e Architettura
----

Facing the biodeterioration of construction and cultural heritage materials:
a novel approach to predict algae growth on fired brick surfaces

Ph.D. Dissertation of:

Benedetta Gregorini

Advisor:

Prof. Marco D'Orazio

Coadvisor:

Prof. Enrico Quagliarini

Curriculum supervisor:

Prof. Francesco Fatone

XIX edition - new series

alle donne forti
e agli uomini
che stanno loro accanto.

Acknowledgments

ii

Abstract

Biodeterioration is the degradation process caused by biological agents and their consequent colonization of surfaces. For cultural heritage materials, especially for fired brick surfaces, this process is recurrent, and it often causes a serious loss of cultural value, as well as economic due to the frequently required maintenance operations. In addition, hazard for human health can arise due to the microbial activities. Fired bricks in building construction are often colonized by microorganisms such as algae and cyanobacteria, which also act as a trailblazer for all other biological forms. This happens because the substrate characteristics (i.e. porosity and roughness) in combination with the environmental conditions, e.g. temperature and relative humidity, allow the retention of water inside the material and offer mechanical grips, ensuring favorable conditions for the development of microalgae. Numerous mathematical models describing microbial growth on building surfaces have been provided in recent years aiming to reduce the decay of the surfaces and to prevent risks for human health. Such models are capable to simulate biofouling (mainly for mold and fungi) on different building materials (e.g. wood, concrete, plasters and even on insulating materials). Moreover, thanks to their analytical formulation, they were implemented on heat and moisture transport simulation software allowing engineers and practitioners to forecast biofouling on building components over years. Conversely, models for algae and cyanobacteria are still limited, to the author's knowledge. Therefore, this work wants to be part of this trend by providing a novel approach aimed at simulating, predicting and, thus, preventing biodeterioration phenomena due to algae growth on fired brick surfaces. Such approach firstly provides the definition of an algae growth failure model starting from influencing factors of the materials and environmental conditions. The model is preliminary developed through the implementation of the Avrami's equation and it is based experimental data on bricks The model is then implemented to predict algae growth under time-varying environmental conditions (time history) so as to allow future application on heat and moisture transport simulation software. The model is based on the Avrami's theory because literature has widely applied it over the years: it was used to describe algae biofouling on mortars, bricks and stones under optimal and non-optimal environmental conditions, and even when considering biocides surfaces treatments. Despite that, some flaws have been detected from both the experimental and analytical side. Due to these limitations, the second aspect of the novel approach wants to provide a new theory overcoming these flaws. The chosen theory is the logistic equation since it was developed and now widely adopted in describing general population growth processes. Hence, a theorical comparison between the Avrami's theory and the logistic equation is performed concerning the ability of (1) overlapping the experimental data, (2) overcoming Avrami's flaws and (3) the correlation with the algae growth influencing factors. The results of this work confirm the capabilities of both of the strategies. The failure model for algae growth is determined and validated for fired bricks surfaces and then its applications show its wide range applicability, such as to different type of bricks, temperature and relative humidity values, both constant and variable over the time. However, the formulation of the model based on the Avrami's theory can be implemented with the logistic formula since it has been proven to be more performing, and hence allowing the application of such strategy to different populations.

iv

Contents

List of figures

Main Text

Appendix A

Appendix B

List of tables

Nomenclature

Avrami's and Logistic Theory	
Experimental parameters	
X	covered area by algae biofouling [-]
A_C/A_T	parameter of final covered area ratio [-]
K	parameter of growth rate [-]
t_l	parameter of latency time [day]
n	Avrami's exponent [-]
r	parameter of intrinsic growth rate [day^{-1}]
t_p	parameter of flex point time [day]
The Empirical Failure Model	
Fitted parameters	
$X\,(P, R, A, T, RH, t)$	covered area by algae biofouling [-]
$A_C/A_T\,(P, R)$	parameter of final covered area ratio [-]
$K\,(P, A)$	parameter of growth rate [-]
$t_l\,(R)$	parameter of latency time [day]
$\tau_A\,(P, R)$	scale function of temperature on A_c/A_t [-]
$\tau_K\,(P, R)$	scale function of temperature on K [-]
$\tau_{t1}\,(P, R)$	scale function of temperature on t_l [-]
Ω	scale function of relative humidity [-]
Variables	
t	time [day]
P	total porosity [%]
R	roughness [μm]
A	total pore area [m^2/g]
T	temperature [°C]
RH	relative humidity [%]
Coefficients	
$a, \ldots, v$	regression coefficients [-]
$\alpha, \ldots, \mu$	corrective coefficients [-]

ALGAE Failure Model	
Fitted parameters	
$X\,(t,\,T,\,RH,\,P,\,R)$	covered area by algae biofouling [-]
$A_C/A_T\,(T,\,P,\,R)$	parameter of final covered area ratio [-]
$K\,(T,\,P,\,R)$	parameter of growth rate [-]
$t_1\,(P,\,R)$	parameter of latency time [day]
Variables	
t	time [day]
T	temperature [°C]
RH	relative humidity [%]
P	total porosity [-]
R	roughness [µm]
Coefficients	
Ω	relative humidity on-off factor
$t_{s,i}$	time shift for i-th time interval [day]
a	temperature cubic equation coef. for A_C/A_T parameter [-]
b	temperature cubic equation coef. for K parameter [-]
c	temperature cubic equation coef. for t_1 parameter [-]
$\alpha,\,\beta$	n-grade polynomial regr. coef. of material prop.
Subscript and Superscript $_P$	
$_P$	porosity index for temperature coefficients
$_R$	roughness index for temperature coefficients
$_n$	number of temperature a-coefficient, from 0 to 3
$_j$	number of coefficient/exponents for porosity
$_k$	number of coefficient/exponents for porosity

Chapter 1

Introduction

The biodeterioration of building materials is a long-discussed and debated problem in the scientific research world [1–3]. This is because the degradation and deterioration of the affected surfaces cause high repair and maintenance costs and loss of cultural value, when they occur on cultural heritage materials [4–6]. Lastly, recent studies have also shown that the presence of microorganisms (i.e. molds and fungi) in indoor environments has significantly affected the quality of the air [7]. Due to the volatility of organic compounds and some pathogens, hazards to the health of the occupants such as allergies and respiratory problems were also found [8,9].

Fired bricks are one of the most common materials in the construction world since Roman and Egyptian times thanks to the availability of raw materials, the versatility of application and installation (e.g. bricks, roof tiles, floor tiles and cladding) and their low cost [10,11]. Durability and resistance to decay drivers are also a fundamental characteristic of this type of material. Nevertheless, they are highly subject to biofouling and degradation resulting from the activity of microorganisms due to their high roughness and porosity resulting from the production process [12–14]. It has been widely recognized that roughness offers a mechanical grip that favors the deposition of microorganisms while porosity allows water to stagnate in the material and therefore provide nutrients to microorganisms [10,15,16].

Among the microorganisms that make up the biofouling of bricks, the main actors are green microalgae and cyanobacteria which also act as a forerunner for the ecological succession of other organisms such as molds, fungi, bacteria, actinomycetes, etc [1,5,6,17]. Their great adaptability allows them to take root on different materials under different environmental conditions, up to survive even in extreme conditions [18–20]. For building materials and in particular for bricks, it has been seen that algae are able to grow at different temperatures on different types of substrate [16,21–25]. However, a necessary condition for starting the growth is that there is liquid water: without that, no visible signs of growth were found [20,25].

For algae growth, literature has so far identified the Avrami's theory as the theory that best describes the development of algae biofouling on building materials. In fact, firstly developed for mortar [26], it has been then applied to various bricks and stones, with or without biocidal treatments and also with growth conditions different from the optimal ones [15,25,27,28]. The results show that Avrami's theory has good reliability in modeling experimental data, even if it fails in describing very rapid growth processes and it shows an analytical bug[15]. On the other hand, the theory based on the logistic equation has never been applied in order to simulate algae growth on building materials, but it was frequently adopted to describe growth process for other type of population under several conditions [29–31]. Despite the limitation of the Avrami's theory, a first empirical model for algae growth has been recently developed on such theory [32]. This work arranged such model by firstly identifying the

factors that influence the growth for both the substrate and for the environmental conditions and then by determining a first set of equations based on iterative fitting process of experimental data. It is based on fired bricks and stones [32]. Having a simulation tool for algae growth on bricks and subsequently on all other porous building materials (e.g. stones, mortars and plasters) thus becomes a key factor in reducing maintenance costs due to biodeterioration and forecasting the risk of exposure to related pathogens agents [33–35]. As proof, it can be noted that in the last decades numerous prediction models of mold growth (i.e. VTT model, isopleth, WTA) have been developed and widely implemented in heat and moisture transfer simulation software [29,36–41].

Therefore, the aim of this work is to develop a novel approach for modeling and predicting algae growth, starting with fired brick surfaces. Firstly, such approach provides the development of a failure prediction model based on Avrami's theory. The model must fulfil these requirements: (1) predictive, i.e. the model must be able to calculate the growth curve starting from a set of input values, even considering the time-varying ones such the environmental conditions, that represent the influencing factors for algae; (2) generally applicable to building bricks; (3) easily implementable and compatible with hygrothermal simulation software outputs such temperature and relative time histories files. The Avrami's theory that stands at the basis of the model is considered sufficiently correct, despite some limitations, as a response to the urgent need of a prediction model. Subsequently, the approach developed in this work also includes the identification of a new basic theory that can describe algae growth and overcome Avrami's flaws. Consequently, this work compares this latter theory with the logistic formula, identified by numerous studies as adequate to describe the growth of a population, both for micro and macroorganisms. This new basic theory will allow, in the future, the definition of a model that may be truly capable of describing algae growth under all growth conditions.

This thesis is hence divided in 8 chapters. The first chapter (Chapter 2) discuss the problem of algae biofouling and its deterioration phenomena, while, Chapter 3 and Chapter 4 deepen the theories and the existing failure model for algae growth. Then, the requirements, experimental data and fitting methods for the development of the model are presented in Chapter 5. The methods for the comparison of the logistic formula to the Avrami's theory are described in Chapter 6. Eventually, the results section in Chapter 7 shows the equations and coefficients for the model and its application to different scenarios, while Chapters 8 reports the results of the comparison between the basic theories of the model.

Chapter 2

Biodeterioration of building materials

2.1 Construction and cultural heritage materials and their bioreceptivity

Bricks and stones are two of the most important materials traditionally used for both construction and decorative purposes and even most of the worldwide cultural heritage monuments are constructed using these porous material [2,3]. Natural and man-made stone materials (concrete, brickwork, mortar) of different structures, textures and colors are used to achieve the physical and technical requirements required by engineers and architects in order to guarantee aesthetic, artistic values and above all structural issues [42]. They were, and still are, commonly applied for both structural purposes (i.e. masonry construction) and as secondary element, such as tiles used for roofing, flooring and cladding purposes [10].

In particular, the use of brick as a building material dates back to antiquity and has continued throughout history until present [43]. Their selection for construction purposes is motivated by questions of durability, availability, workability, cost and appearance. Among them, workability, cost and installation speed play a crucial role in the use of ceramics when compared to stone, especially due to the ease and economy of forming raw ceramic materials. Sun-dried clay bricks were used for construction, but with the passage of time, these started to be fired to enhance their resistance [11].

Both fired bricks and stones are characterized by a wide range of mineral composition and different type of microstructure. Therefore, the physical, mechanical and chemical properties of such materials are extremely variable, resulting in widely different abilities to resist weathering and degradation (durability) [13,44]. Since fired bricks are a man-made product, their properties (e.g. composition, texture and porosity) are also strictly linked to the raw materials composition and granulometry and affected by the firing temperature and production cycle to which they were subjected [12,44,45].

Besides the standard materials properties (e.g. physical, mechanical and chemical ones), these characteristics can influence the bioreceptivity of the material itself. Bioreceptivity implies an ecological relationship between the substratum and the colonizing organisms and it was firstly defined as "the aptitude of a material to be colonized by one or several groups of living organisms without necessarily undergoing any biodeterioration" or as "the totality of material properties that contribute to the establishment, anchorage and development of fauna and/or flor" by Gullitte in 1995 [14]. As the intrinsic characteristics of the stone materials can change over time as a result of exposure to degradation phenomena, bioreceptivity cannot be considered as a static property and, hence, three type of bioreceptivity can be defined for each material according to the different stages of deterioration. These three steps of bioreceptivity are defined as [14]: primary or intrinsic bioreceptivity, which is related to the initial potential of biological colonization of sound stone, secondary bioreceptivity, which refers to the potential of biological colonization of

weathered stone, and tertiary bioreceptivity, which is the colonization potential of a stone material subjected to conservation treatments. Lastly, particles or substances that are not part of the material, such as soil. dust, organic particle, water stagnation, can deposit and, in combination of the properties of the material itself, they can accumulate biological substances: this phenomenon can be defined as semi/extrinsic bioreceptivity. For stony and fired brick materials, it relates mainly to petrochemical characteristics and petrophysical properties such as: pore space structure (e.g. porosity, permeability, capillarity kinetics) and surface roughness [46]. In parallel, the design of the building itself can affect the semi extrinsic bioreceptivity of fired bricks and stones: defect in water pipes, north orientation, shading, traffic exposition can promote the deposition of microorganism on the material and subsequently favor their growth [10,12,47,48].

2.2   Biofouling phenomenology and biodeterioration effects

Biofouling, or biological fouling, is the process of accumulation of microorganisms, such algae, bacteria and fungi, and macroorganisms i.e. plants, lichens and musk on building materials [4,28]. By adhering to the surfaces, they form biological stains, patinas and crusts that can vary in extent, thickness consistency and color [6]. The former three are easily influenced by the material type, the building design and surrounding environmental conditions. Color, on the other hand, is mostly varying between green, grey and black and it is depending on the type of the microorganism [49–52].

Biodeterioration is, therefore, the collection of any undesired change in material properties caused by the activities of such living organisms [48]. Biodeterioration phenomena may be grouped broadly into three categories: biophysical, biochemical, and aesthetic deterioration. Depending on the biodeteriogens, on the material type and on the environmental conditions, these processes may occur separately or simultaneously [6,53]. Moreover, apart from the direct actions, the development of biofouling can create conditions favorable to the growth of other species (e.g. mold, fungi, mosses, lichens) and, hence, an ecological succession [1]. Among the harmful effects of biofouling, the main one is the aesthetic damage. In fact, patinas, stains and consequent incrustation can alter the color of the material and the surface finishing layer [4,6]. The aesthetic damage itself does not affect the conservation of the material or the stability of the building itself but can cause a loss of cultural value, if the building is provided with it, and of economic value due to the continuous maintenance operation required [54–56].

Another effect of biodegradation, less recognizable, but often more harmful than the aesthetic one, is the mechanical, physical (i.e. disintegration) and chemical (i.e. decomposition) damage caused by the interaction of microorganisms with the surface of the material [1]. They produce a large variety of metabolites like polysaccharides, proteins, peptides, amino acids and other organic acids like fatty acids. These acids either actively dissolve stone constituents or increase their solubility in water and stimulate migration of salts in stone, causing powdering of its surface. These processes can affect the material properties resulting in loss of surface cohesion of the material and in transformation and dissolution of the components of the material [17]. Once the surface is weekend by the action of the metabolic activity of microorganisms, more severe mechanical breaks and physical stress can happen in a synergetic combination with other external agents such the outdoor weather (rain, wind,

sun, freeze/thawing cycles) and human activities related agents (e.g. acid rain, traffic vibration and pollution) [5,57].

Finally, the presence of mold and fungi among the microorganism can affect the indoor air quality of the buildings and represent a threat for human health [7,58]. In fact, they can produce contaminants, i.e. volatile organic compound such as spores, allergens, toxins and other metabolites or they can deposit pathogens and subsequently spread them in the indoor environment. The most significant health dangers experienced by exposed people include irritations and toxic effects, superficial and systemic infections, allergies and other respiratory and skin diseases [9]. The extent of exposure to these microbial airborne particles and the associated risks are related to many parameters, such as genera/species of microorganisms (which determine a part of the contaminants), exposure pathway (inhalation or contact with skin/eyes) and environmental conditions (convection, etc.), total area of microbial growth, aerosolization of contaminants, etc [8].

2.3 Algae and Cyanobacteria as main actors

Among inorganic materials such as bricks used in the construction world, the first microorganisms that initiate biofouling are the autotrophic ones [5]. These organisms in fact have the ability to take root, grow and develop by transforming the inorganic resources at their disposal on the material (such as CO_2, water and nitrates) into complex organic nutritive compounds by exploiting the sunlight [1]. Autotrophic organisms that can be found in building materials are bacteria, actinomycetes, molds, fungi and a combination of algae and cyanobacteria [1,5,6,17].

If bacteria, in particular actinomycetes, are frequent in underground environments characterized by poor lighting and high relative humidity [56,59,60], microalgae and cyanobacteria are classified as the first colonizers of the building envelope [61]. This happens due to their three fundamental characteristics: ease of engraftment, adaptability to different substrates and ability to survive even to extreme environmental conditions.

The first one is due to the fact that the necessary condition, but also sufficient, for the spores and cells of microalgae and cyanobacteria to colonize a material is that there is light, water and some readily available inorganic components (CO_2, nitrates and traces of mineral salts) [62]. A significant case is the appearance of algae in an underground environment (Moidons Cave, France) where due to the installation of an ambient lighting system, the spores of algae brought from outside have taken root easily [63–65].

Subsequently, these organisms can adapt themselves to very particular substrata, changing in color and morphology. Cyanobacteria and green algae were found on several materials types: concrete and stones, fired brick, and even metals, painted surfaces and plastic [18].

Finally, the combination of the filamentous structure of the microalgae and the more or less thick gelatinous sheath layer formed by the cyanobacteria allows such them to trap, absorb and therefore retain water [1]. In combination with the fact that they are also capable of activating and deactivating the metabolism, these microorganisms are able to resist even extreme fluctuations in environmental conditions and therefore live even in the most extreme terrestrial climates, such as hot and cold deserts [19,20].

Among the species of algae and cyanobacteria, two of the most recurrent in building materials are *Chlorella mirabilis* for green algae and *Chroococcidiopsis fissurarum* for cyanobacteria

[66]. In relation to the substrate and the environmental conditions these two species produce stains and patinas often leading to green, gray and black colors, although red and brown spots can also be found when combined with other algae species [1,5,6,17]. In addition to the aesthetic damage, however, the researchers found that algae contribute to bricks, and more generally stones, deterioration by respiration processes, by retaining water which expands in freeze-thaw cycles or by releasing acids or chelating compounds [4]. In addition to acids, many other organic compounds (e.g., amino acids and polypeptides) are also able to complex or chelate ions. Due to this, the film they produce allows the engraftment of other microorganisms, both autotrophic and heterotrophic (such as plants) [18].

2.4   Factors influencing algae biofouling on fired bricks

The identification and clear determination of which are the main factors influencing algae growth on porous building materials, in particular on bricks, is a key factor for properly describing the algae growth and, therefore, for simulating it correctly through a predictive model [67,68]. However, this has caused, and still does, discussions among researchers. In fact, it is not easy to understand what are the primary and strictly influencing factors due to the numerous and different species of algae, the various types of substrate and the disparate environmental conditions for which algae biofouling took place [62,65,69]. In any case, all the factors must ensure water and nutrition for algae. If there is no available water or nutrients at the engraftment time, the algae are unable to develop [5,51,62,69].

As for the substrate made up of porous construction materials, the bioreceptivity of the material certainly influences the growth and development of algae and, specifically, the petrochemical characteristics and petrophysical properties play a primary role [10,14,46]. Numerous studies and laboratory tests conducted in this regard have identified how roughness and porosity are two factors strictly influencing growth and development [13,15,16,21,26,70–72]. The first, in fact, allows the mechanical anchoring of the microalgae spores and filaments present in the air [21,71,72]. The second, on the other hand, is closely related to the water availability as it helps the retention of water within the material and it extends its availability over time [5,10,12,13]. On the other hand, factors such as pH and the mineralogical composition of the materials, both for bricks and stones, seem to have only secondary and not well-defined effects in the development process [12,13,48,73]. In fact, literature has largely proven that algae are able to grow on surfaces with different pH without absorbing their effect, while, the chemical composition of the substrate is secondary algae growth, because it is not directly linked to the water availability [12,13,48,73].

Among the environmental conditions, temperature and relative humidity have been recognized as primary factors in algae growth [74]. Indeed, recent studies have identified relative humidity and the presence of water in conditions close to saturation as an on-off condition for algae growth [20,25]. Only if the relative humidity and the water content in the material are close to saturation (≥98%) there are visible signs of algae growth on building bricks. However, if the algae were able to start their growth and develop, a lower relative humidity only blocks their development but does not lead to their death [19,20]. In fact, it has been shown that algae are able to retain water inside them, deactivate the metabolism and therefore survive even dry periods [1]. Regarding temperature, the scientific literature has identified optimal ranges for which growth occurs and has defined minimum and maximum

6

boundary values in which growth does not occur or stops [74]. In general, for most algae and cyanobacteria a range of temperature where growth occurs is between 20° C and 30° C, while between 5° C and 40° C growth stops [20,75–77]. Nevertheless, it is possible to find stains or patinas caused by algae biofouling above these limit temperatures as these microorganisms have the possibility to adapt and survive [78]. Currently, the correlation between these 4 influencing factors has been made only qualitatively by identifying that porosity and roughness influence the development time and partly the covered surface, while T and RH strongly influence algae growth in terms of activation and development of biofouling [25]. Finally, even the building design can have an effect on algae growth since it affects, more or less directly, the water availability of inside the materials [79]. For example, in addition to wind driven rain and rising damp, it was also found that the north orientation and shading slow down evaporation and favor the stagnation of the water content inside the material [17,20]. In addition, both external and internal insulation can also promote algae growth as they reduce the temperature of the wall, making it reach the dew point and favoring condensation phenomena [80,81]. Finally, even inadequately designed parts of the building (e.g. balconies and ledge) or defects in water regulation can create preferential routes where the water accumulated after a rain event stagnates, creating the ideal conditions for the proliferation of algae and cyanobacteria [79,82,83]. Figure 2.1 show some examples of substrate properties, environmental conditions and defect in the building design that favored algae growth.

Figure 2.1 Different combination of fired bricks substrates, environmental conditions and building design details leading to algae growth.

Chapter 3

Theories describing algae biofouling

3.1 The Avrami's theory and its flaws in simulating a rapid growth

Concerning theories for describing algae growth, scientific literature over the past few years has provided some attempts: the first models suggested the solution of differential equations and network models to describe the algae growth from the pore-scale to the macro scale [84–87], while the most recent models proposed the use of modern machine learning technologies and artificial neural network to take into account more variables, such as those of the substrate, which can influence the growth [88,89]. But such models has found only limited application on describing the algae biofouling on building materials: that is probably due to difficulties in determining the parameters, solving the equations and/or high costs in computations (e.g. due to the use of machine learning technologies).

The Avrami's theory, on the other hand, has been developed only recently but it is the most widespread model for describing algae growth applied to building materials. In fact, this theory was originally developed to describe the kinetic phase transformations in solids [90–94], but since solid nuclei and algae spot could be easily compared given some assumption [26,95], the theory has been rapidly applied to algae growth on building material. As nucleation and growth for solid, such growth over the time can be respectively discretized in three phases [26,95]. The first is the latency time, corresponding to the nucleation, in which the algae spots start colonizing the substrate, but they are not still visible to naked eye. Then, the exponential growth occurs similarly to the nuclei growth, and the substrate is rapidly covered by algae fouling. Finally, the stagnation phase takes place, and it is when the algae growth becomes stable over the time due to the unavailability of novel resources. The first applications of the model has taken place on mortars with Portland cement where algae growth reach the saturation of the area [26]. Subsequent changes to the initial formulation (modified Avrami's model) allow the application of the model even where the algae are not able to reach total coverage, while maintaining the sigmoidal shape of the output curve [27,28]. This has promoted the extension of the applicability of the model to materials that are only partially favorable to algae growth (i.e. slightly porous and slightly rough fired bricks surfaces) [15,27], materials treated with biocides [15,27,28] and when the environmental conditions can limit their development (e.g. low temperature) [25].

The Avrami's theory, with its implementation resulting from different application, is presented in (1)

$$X(t) = \frac{A_C}{A_T} \cdot \left(1 - \exp^{-K(t-t_1)^n}\right) \tag{1}$$

where the covered area by algae growth X(t) [-] is defined by an exponential equation depending on the time of growth t [day]. The final covered area ratio is represented by the parameter A_C/A_T [-] which expresses the maximum percentage of the covered area at the end of the process (A_C is the covered area by algae at the end of the accelerated growth test, and A_T is the total area of the sample) and it can range between 0 and 1. The K [-] is a growth rate parameter depending on the rate of the nucleation of new particles, and the specific growth rate constant [27,28] and it can be determined by the least squares method using experimental measurements [28]. Lastly, the parameter t_l represents the latency time [day] before a chromatic variation occurs on the material surface: it can be assumed as the comparisons of the first algae spot. The dimension of the spot can be reasonably approximated to 0.003, since it is the area of one pixel in a sample of 80 x 80 mm^2 with an image resolution of 600 dpi [27,28]. The coefficient n is the Avrami's exponent for the time variation and it is assumed equal to 4, with three dimensions representing the growth and one representing a constant nucleation rate [28]. All the four parameters can be assumed constant over the time but, by the determination of the parameters A_C/A_T, K and t_l, it is possible to adapt the curve to the experimental data so as to model the various materials. This function has a minimum value equal to 0, when the time t corresponds to the latency time t_l, while it does not have a maximum value (it asymptotically tends to A_c/A_t for t→∞).

However, 2 important limitations of such theory can be pointed out. A previous work [15] highlighted that one of the Avrami's flaws occurs when the growth rate is very fast (i.e.: on materials having high porosity and/or high roughness) and the latency phase is very missing. Since the curve has a minimum value equal to 0 (when the time t corresponds to the latency time t_l) that prevents the curve to develop as fast as the experimental microalgae biofouling, or consider in some ways the effect of algae inoculationFigure 3.1shows the Avrami's curve failing in describing such growth process [15].
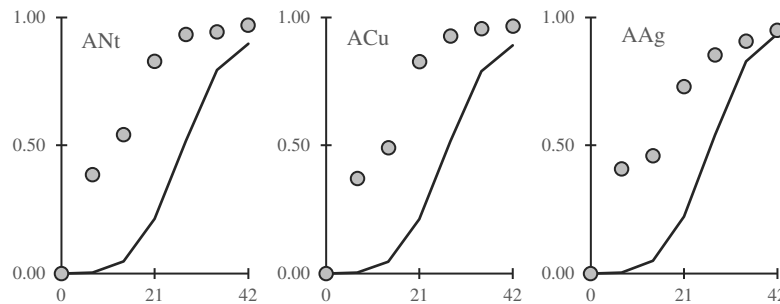
Figure 3.1. Avrami's flaws in describing a very rapid growth, with a latency time almost equal to 0 for literature materials [15].

The second limitation, conversely, occurs when the latency time extends over the growth time, e.g. for materials with low porosity and/or roughness but it can be considered as a mere analytical bug. In fact, according to the first derivative (2),

10

$$X'(t) = 4 \cdot \frac{A_C}{A_T} \cdot K \cdot -\exp^{-K(t-t_1)^4} \cdot (t-t_1)^3 \le 0, \; \forall t \le t_1 \tag{2}$$

such model shows a decreasing trend for every $t \le t_1$, since the other parameters (i.e. the covered area ratio A_C/A_T and the growth rate factor K) are higher or at least equal to 0 [25]. The miscalculation of the predicted biofouling is rather poor, and the affected interval is usually very short if compared to the total growth time. Despite that, the effect of the miscalculation is not so correct for physical description of microalgae growth.

3.2   The logistic model for general population growth

Differently to Avrami's theory, that was initially developed for nucleation solids and only later applied to algae growth, the logistic formula was developed and directly applied for population growth description. One of the first application was for describing human population growth, but rapidly it has been extended to biological growth, medicine and its generalized version has been even applied for COVID-19 modeling [30,96–99].
For what concerns algae growth, the use of logistic formula is quite spread i.e. for the biofuel industry [99,100]. Numerous studies have adopted this formulation to simulate the experimental data of in vitro cultivations, often comparing them with other mathematical models for growth prediction [31,100–103]. The results obtained in these scientific studies have identified the logistic function as the most suitable model for the representation of the experimental data [104]. Concerning the description of biofouling on porous building materials, the logistic formula has been successfully applied only in a recent study for mold growth [29], but no application for algae growth is known up to now to the authors.
As for the Avrami's model, this equation is based on an exponential formulation of growth, with a starting phase of latency and an ending phase of stagnation, once the maximum exploitation of the resources available for growth has been reached [97]. The logistic function proposed in this work is defined by equation (3), proposed in [29,31]:

$$X(t) = \frac{A_C}{A_T} \cdot \left(\frac{1}{1+\exp^{-r(t-t_f)}} \right) \tag{3}$$

where, microalgae coverage X [-] is a function of time t [day] and the three parameters, namely A_C/A_T, r and t_p, can be defined from experimental measures. In particular, the first one is the maximum covered area ratio [-], being A_C the area covered by microalgae and A_T the total area of the sample. It represents the horizontal asymptote ranging between 0 and 1. The r parameter [day^{-1}] can be defined as the intrinsic growth rate [31] while the t_p parameter [day] is defined as the inflection point of the growth curve and it is the day in which microalgae coverage $(A_C/A_T)/2$ is reached. It is analytically determined by setting the second order derivative of logistic function equal to zero [31]. At time 0, the microalgae coverage can range between 0 and $(A_C/A_T)/2$ due to the definition of t_p. This overestimation of the zero starting point has been previously considered as acceptable, describing the effect of microalgae inoculation [31,101,104]. Both r and t_p are calculated through iterations by

11

minimizing the least squares value between experimental data and calculated values [31]. Moreover, the model first derivative is always higher than 0 for every time values (4):

$$X'(t) = \frac{A_C}{A_T} \cdot \frac{r \cdot \exp^{-r(t-t_p)}}{\left(1+\exp^{-r(t-t_p)}\right)^2} \geq 0 \quad \forall t \tag{4}$$

being A_C/A_T, r and t_p are always higher or at least equal to 0 due to their experimental definition, Hence, no decreasing trend can be observed as happening for the Avrami's laws

Chapter 4

The first empirical model for algae growth from literature

4.1 Looking to other existing models for biofouling on building materials

In order to describe and therefore limit biofouling risk that may damage the building itself or just a part of it (e.g.: walls, façades, wooden beam ends), in recent years researchers have been providing several failure models [29,36–38]. From an engineering point of view, a correct modeling of the biofouling phenomenon can provide to engineers and practitioners a useful tool both for predicting the damage on the various building materials and for the correct planning of maintenance interventions so as to be able to limit their costs [33–35].

A failure model is mathematical model capable of describing risks and decay starting from the influencing factors of biofouling [33]. Several prediction models were provided differing from each other depending on the considered microorganisms (e.g. mold, fungi, algae, actinomycetes), the considered input parameters (e.g.: temperature, moisture, exposure time and substrate type and properties) and the type of given output (i.e.: static model, when the output indicates the starting of the process, and dynamic model that can describe the overall process considering both the starting and the decline generally as a function of time) [29,36–38,67,68].

Since mold and fungi can easily growth in the indoor environment when the relative humidity is just higher than 80% and, concurrently, they can cause hazards to human health, numerous failure models have been provided. The first development started considering the temperature ratio according to which a temperature ration lower/higher than 0.7 would provoke relative humidity higher than 80% and, hence, an unacceptable high mold risk [105]. Subsequently, models were implemented considering minimum combination of temperature and relative humidity in which growth occurred and some a first implementation of such models on hygrothermal software was provided [58,106,107].

Then, the VTT model introduced also the substrate properties as influencing factor for mold growth. At first, in order to determine the Mold Index, only two type of wood (pine and spruce) and two type of finishing (resawn and original kiln-dried) were considered [107,108], but such classifications were enlarged in order to consider more materials and hence scenarios. In particular, different types of building materials were added (i.e.: spruce, concrete, PUR thermal insulation, glass wool and EPS) being grouped in their mold growth sensitivity classes (i.e. very sensitive, sensitive, medium resistant and resistant) [7,38,109].

In recent years, the VTT model and the WTA model have been finally implemented on heat and moisture simulation software such as DELPHIN (http://www.bauklimatik-dresden.de/delphin/index.php , last access: December 2020) and WUFI (https://wufi.de/en , last access: December 2020). Both software are able to calculate the temperature and relative

humidity profile for a given building component, in particular façades and roofs, according to their material composition (e.g. type of insulation, type of finish, materials thickness, etc.). Starting from this, it is therefore possible to obtain also the profile of temperature and relative humidity over time (that is time history files) and then apply them on the calculation of the models. Hence, engineers, researchers and practitioners are able to simulate the decay and degradation due to biofouling [39–41].

4.2 Theory and equations

In order to provide a failure model capable to simulate biofouling directly starting from the substrate properties and environmental condition of the building constructions, avoiding background experimental tests [33,67], a first attempt for algae growth on building materials has been provided by [32]. The empirical failure model provided by literature [32] is presented in equation (5):

$$X(P,R,A,T,RH,t) = \Omega \cdot \tau_A \cdot \frac{A_C}{A_T} \cdot \left[1 - \exp^{-(\tau_K \cdot K)\left(t - \tau_{t_1} \cdot t_1\right)^n} \right] \tag{5}$$

where the algae growth is a function of substrate properties (i.e. porosity P [%], roughness R [µm] and total pore area A [m²/g]), environmental conditions (i.e. temperature T [°C] and relative humidity RH [%]) and time t [day] [32]. The model is suitable for both bricks and stones.

The substrate properties variables were directly expressed in the Avrami's parameter calculation A_C/A_T (P, R), K (P, A) and t_l (R), expressed in condition (6) [32].

$$\begin{cases} \dfrac{A_C}{A_T}(P,R) = 1 - \exp^{-\alpha\left(2.48 \cdot P + 0.126 \cdot R\right)^4} \\[2em] K(P,A) = 1 - \exp^{-\beta\left(\dfrac{4.49 \cdot 10^{-3} \cdot P + 4.49 \cdot 10^{-3} \cdot A + 5.79 \cdot 10^{-3}}{2.09}\right)^2} \\[2em] t_1(R) = \gamma \dfrac{5}{(R-5.02)^2} \end{cases} \tag{6}$$

14

The temperature is considered as a scaling effect on such parameters and hence computed as $\tau_A(T)$, $\tau_K(T)$ and $\tau_{t1}(T)$ [-], while relative humidity has a general on/off effect on algae growth determined as $\Omega(RH)$ [-] according to conditions (7) [32].

$$\begin{cases} \tau_A(T) = r_A \cdot T^3 + s_A \cdot T^2 + u_A \cdot T + v_A \\[2ex] \tau_K(T) = r_K \cdot T^3 + s_K \cdot T^2 + u_K \cdot T + v_K \\[2ex] \tau_{t_1}(T) = 1 \\[2ex] \Omega(RH) = \begin{cases} 0, & RH < 98\% \\ 1, & RH \geq 98\% \end{cases} \end{cases} \tag{7}$$

Since both the scale functions τ_A and τ_K experimentally determined have shown a correlation with the substrate properties (P, R), the regression coefficients equation based on such variables $(a^I, b^I, \ldots, d^{IV})$ are determined according to conditions (8) and (9) [32].

$$\begin{cases} r_A(P,R) = \delta_A \left(a^I \cdot P + b^I \cdot R + d^I \right) \\[2ex] s_A(P,R) = \eta_A \left(a^{II} \cdot P + b^{II} \cdot R + d^{II} \right) \\[2ex] u_A(P,R) = \lambda_A \left(a^{III} \cdot P + b^{III} \cdot R + d^{III} \right) \\[2ex] v_A(P,R) = \mu_A \left(a^{IV} \cdot P + b^{IV} \cdot R + d^{IV} \right) \end{cases} \tag{8}$$

$$\begin{cases} r_K(P,R) = \delta_K \left(a^I \cdot P + b^I \cdot R + d^I \right) \\[2ex] s_K(P,R) = \eta_K \left(a^{II} \cdot P + b^{II} \cdot R + d^{II} \right) \\[2ex] u_K(P,R) = \lambda_K \left(a^{III} \cdot P + b^{III} \cdot R + d^{III} \right) \\[2ex] v_K(P,R) = \mu_K \left(a^{IV} \cdot P + b^{IV} \cdot R + d^{IV} \right) \end{cases} \tag{9}$$

Table 4.1 shows the regression coefficients a^i, b^i and d^i of conditions (8) and (9) that, as a result of the fitting process, assume significant values. In general, all the regression coefficients of the τ_A and τ_K scale functions, respectively r_A, s_A, u_A, v_A and r_K, s_K, u_K, v_K in equations (8) and (9), have resulted significant [32].

Regression coefficient	P	R	Constant term
r_A	$a^I = 3.8447 \cdot 10^{-4}$	$b^I = -4.0800 \cdot 10^{-6}$	$d^I = -2.1164 \cdot 10^{-4}$
s_A	$a^{II} = -2.7874 \cdot 10^{-2}$	$b^{II} = 2.9590 \cdot 10^{-4}$	$d^{II} = 1.1856 \cdot 10^{-2}$
u_A	$a^{III} = 5.5270 \cdot 10^{-1}$	$b^{III} = -5.8670 \cdot 10^{-3}$	$d^{III} = -1.4727 \cdot 10^{-1}$
v_A	$a^{IV} = -2.1146$	$b^{IV} = 2.2450 \cdot 10^{-2}$	$d^{IV} = 4.7041 \cdot 10^{-1}$
r_K	$a^I = 8.3270 \cdot 10^{-5}$	$b^I = 6.7000 \cdot 10^{-7}$	$d^I = -1.8459 \cdot 10^{-4}$
s_K	$a^{II} = -6.0378 \cdot 10^{-3}$	$b^{II} = -4.8800 \cdot 10^{-5}$	$d^{II} = 9.8770 \cdot 10^{-3}$
u_K	$a^{III} = 1.1971 \cdot 10^{-1}$	$b^{III} = 9.6900 \cdot 10^{-4}$	$d^{III} = -1.0759 \cdot 10^{-1}$
v_K	$a^{IV} = -4.5803 \cdot 10^{-1}$	$b^{IV} = -3.7100 \cdot 10^{-3}$	$d^{IV} = 3.1809 \cdot 10^{-1}$

Table 4.1. Regression coefficients determined for the substrate variables (P, R) of the temperature scale functions τ_A and τ_K [32].

The coefficients α, β and γ refer to corrective coefficients according to the material type. Such coefficients are equal to 1 for brick surfaces since the model was primarily determined on bricks but they vary for stony materials [32]. In this way the regression coefficients determined for the A_c/A_t, K and t_1 parameter of fired bricks can be still valid and adequate also for stone substrates. The corrective coefficients (α, β and γ) of the failure models' parameters A_c/A_t, K and t_1 for stones, expressed in equations (6), are shown in Table 4.2.

Parameter	Corrective coefficient	
A_c/A_t	$\alpha = 2$	sandstones
	$\alpha = 100$	limestones
K	$\beta = 1.724$	sandstones
	$\beta = 6.897$	limestones
t_1	$\gamma = 0.2$	sandstones
	$\gamma = 1.6$	limestones

Table 4.2. Calculated values of corrective coefficients for sandstone and limestone materials [32].

Three main hypotheses have been assumed at basis of the model. The first assumption affirms that P, R and A can be reasonably considered as independent variables and not varying over time. That means that they don't depend from each other and from the environmental conditions. Moreover, since they don't vary over the time, aging problem of surface material can be reasonably disregarded. The second assumption involves the environmental conditions: they can be constant, or they can vary over the time. Lastly, the third assumption states that the covered area by algae $X(t)$ is a monotonically not decreasing function. Therefore, even if there aren't suitable environmental conditions for algae growth, the biofouling process cannot go back or decrease. This assumption is supported by the results obtained in previous experimental researches [15,27,28], from which the condition (10) is always valid.

$$X(t_1) \leq X(t_2), \qquad \forall t_1 < t_2 \tag{10}$$

According to the above hypotheses, the failure model manages to simulate the algae growth on a specific building material, taking into account also the environmental conditions. For environmental conditions that remains static over the time, the model is able to analytically determine the curve. On the other hand, when dynamic T and RH are given, a qualitative construction of the model is proposed: once set the substrate properties, the model firstly determines the specific growth curves for the different environmental conditions; subsequently it identifies the sections of the curves related to each time interval; then it combines those section as the overall growth process is the sum of each section. The combination process takes place according to the conservation principle of the reached covered area, through a horizontal asymptote. This implies that a change in environmental conditions results in a variation of the growth rate of the curve. Figure 4.1 shows the curves obtained by the failure model under both static environmental conditions (EC_1, EC_2, EC_3) and dynamic ones (EC_d).
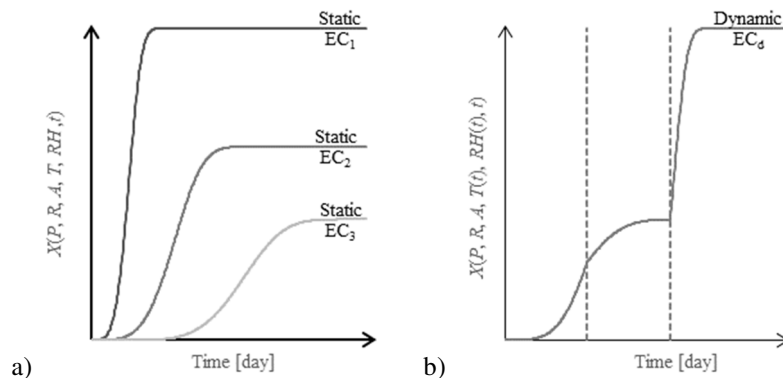
Figure 4.1. Examples of the implemented failure model for a given set of substrate properties: a) analytical determination of the growth curve under static environmental condition; b) qualitative overall process of covered area by algae biofouling under dynamic environmental conditions [32].

17

4.3   Calculation, fitting and validation process

Once set the variables and the parameters to be fitted, the domain and codomain of the failure model have been set. The variables domain is determined according to the experimental and measuring methods, as follow:

- porosity domain – $0 < P < 100$ [%];
- roughness domain – $R \geq 0$ [μm];
- total pore area domain – $A > 0$ [m^2/g];
- temperature domain – $5 \leq T \leq 40$ [°C];
- relative humidity domain – $0 \leq RH \leq 100$ [%].

Moreover, the codomain of the fitted parameter is set according to the mathematical and physical meaning, and considering the experimental results [15,23,27,28,55]; in particular:

- for the final covered area ratio – $0 \leq A_c/A_t \leq 1$ [-];
- for the rate parameter – $0 \leq K \leq 1$ [-];
- for the latency time – $t_l \geq 0$ [day];
- for relative humidity scale function – $0 \leq \Omega \leq 1$ [-];
- for temperature scale functions – $0 \leq \tau_i \leq 1$ [-].

An iterative fitting process is performed in order to obtain the equations and coefficients of the conditions (6)-(9). The tested equation types (e.g. polynomial, logarithmic, exponential, etc) in the fitting process are not decided in advanced nor analytically derived from the Avrami's theory (1). During the fitting process, the resulting equations are considered adequate if they fulfill three requirements. The first states that the equation types must well simulated the trend of the experimental data; the second one requires that the codomain must be verified, while, the third requirement verifies whether the fitting maximizes the coefficients of determination R^2 and minimizes the sums of squared residuals. The iterative process is stopped when all the above three conditions are satisfied. The corrective coefficients ($\alpha, \ldots, \mu$) are determined on the stones experimental data following again the three requirements.

The resulting model is firstly applied to the experimental material, and by overlapping the resulting curves with the average experimental with their relative standard deviation values, is first graphically verified. Then, a quantitative validation is performed by determining the confidential R factor [%] for each material. According to previous literature works [15,27,28], an Avrami's curve with a R factor value lower than 25% can be considered acceptable. Moreover, the validation is performed not only on fired brick materials, but also considering results on stone materials previously investigated [28,55].

18

Chapter 5

ALGAE – ALgae Growth fAilure modEl for bricks

This chapter deepens one of the 2 main goal of the novel approach: the development of a new failure model able to describe algae biofouling on fired brick surfaces.

The model is based on the Avrami's theory because, despite the limitation presented in Section 3.1, it is considered adequately correct, as a response to the urgent need of a prediction model. In addition, the first empirical failure model for algae growth is resumed with the underlying theories and hypotheses (Section 4.2 and Section 4.3) with the aim of improving it, thus, obtaining a failure model.

In fact, according to other failure model already developed for biofouling of building materials (Section 4.1), a failure model as such should be *predictive*, *applicable* and software *implementable*. The predictive requirement means that the model must be able to calculate the growth curve starting from a given set of input values, even considering the time-varying ones such the environmental conditions, representing the factors that influence algae biofouling. Then, it must be generally applicable to fired bricks surfaces, that is, the domain of the substrate input variable should be descriptive of most/all the bricks applied in building construction. Lastly, the calculation method of such model must be easily implementable and compatible with hygrothermal simulation software outputs such temperature and relative time histories files.

Particularly due to this last requirement, this work provides two version of the model: the *static* and the *dynamic* model. These two types of model allow to consider the environmental conditions, in terms of temperature and relative humidity, both constant (hence, static) and varying (dynamic) over the time. In addition, also the calculation processes are slightly different for the two versions considering a user-friendly calculation for the static model and a software determination process for the dynamic one.

Therefore, three section are outlined in this chapter. In Section 5.1, the main theories of the literature empirical failure model are summarized. Then, in Section 5.2 the static model is determined by describing its general requirement, the empirical dataset on which the model is based and the adopted fitting process, Lastly, Section 5.3 defines the dynamic model, describing its basic assumptions and calculation processes.

5.1   Theories and hypothesis from the empirical failure model

The theories and hypotheses according to which the empirical model of algae biofouling is developed are reported as general indications and guidelines that underpin the theoretical basis of the model. The theories resumed from the empirical model are mainly two [32]:

- this new failure model can be still based on Avrami's theory and its subsequent modifications. This is because numerous works of literature have shown the ability

of this theory to describe algae biofouling on several materials, with environmental conditions different from the optimal ones and also when the material surface is treated biocides that inhibited the biofouling [15,25,27,28];

- parallel to the fact that the Avrami's theory constitutes the general equation of the model, the theory of the determination of the three Avrami's parameters with growth influencing factors is resumed from the first model. Such factors are still those describing the effect of substrate and environmental conditions [32].

Simultaneously, all three assumptions underlying the empirical model are recovered for the failure model. The hypotheses are [32]:

- the variables, whether they refer to the substrate or to the environmental conditions, are independent: this is due to both the physical assumptions on such variables and the experimental test program developed for the algae growth data [15,25,27,28];
- the substrate conditions are also independent from time, reasonably disregarding aging problems of the material surface, while temperature and relative humidity are considered both constant and variable over time [15,25,27,28];
- lastly, the third assumption states that the covered area by algae is a monotonically not decreasing function. Therefore, even if there are not suitable environmental conditions for algae growth, the biofouling process can never get back and decrease the covered area [25].

5.2   The static model

5.2.1   General requirement for model definition

The theories and hypotheses derived from the first model are then transformed into analytical conditions that also meet the 3 requirements of the failure model.

The input parameters of the failure model are therefore identified in: open porosity P [-] and surface roughness R [µm] as influencing factor of the substrate and, temperature T [°C] and relative humidity RH [%] describing the environmental conditions. Such variable have been chosen according to the previous model [32], the literature findings [15,25,27,28] and because a failure model needs easily to be measured parameters for having a widespread use. The variable of total pore area A is dismissed for the sake of an easier calculation and implementation: this variable is rarely reported in building material characterization [11,13,15,16,21,22,27,110–114] and more rarely provided in simulation software. Moreover, literature has largely proven that the chemical composition of the substrate plays only a secondary role in algae growth, because it is not directly linked to the water availability, hence, it was not considered [12,13,48,73]. Lastly for what concerns the environmental conditions, it is worth noting that the experimental test apparatus for simulating accelerated growth conditions provided a day/night illumination cycles [25]. In this way, the daily covered area variation measured and adopted for the fitting process of the model takes also into account the day/night illumination cycles. As stated by the theories of empirical model, such variables (porosity P [-], roughness R[µm], temperature T [°C] and relative humidity RH [%]) can therefore modify the algae growth curve of the failure model X (T, RH, P, R, t)

by influencing the three parameters $A_C/A_T(T, RH, P, R)$, $K(T, RH, P, R)$ and $t_1(T, RH, P, R)$. Condition (11) analytically describes such theory:

$$\begin{cases} \dfrac{A_C}{A_T} = \dfrac{A_C}{A_T}(T, RH, P, R) \\[2ex] K = K(T, RH, P, R) \\[2ex] t_1 = t_1(T, RH, P, R) \\[2ex] X(t) = \dfrac{A_C}{A_T}(T, RH, P, R) \cdot \left(1 - \exp^{-K(T,RH,P,R)(t-t_1(T,RH,P,R))^4}\right) \end{cases} \quad (11)$$

Besides, the set given in condition (12) deepens the fact that the algae growth curve over the time is a not decreasing function.

$$\begin{cases} X(t_i) = 0, \forall t_i < t_1 \\ X(t_i) \le X(t_{i+1}), \forall t_i < t_{i+1} \end{cases} \quad (12)$$

The first one involves the latency time and it tried to overcome the analytical inaccuracy. In fact, the use of t_1 led to a miscalculation on the covered area: when the latency time is different from 0, the function showed a decreasing trend between $t = 0$ and $t = t_1$ and, since the function is even, the covered area at $t=0$ was higher than 0. This meant that the growth curve minimum was equal to 0 when $t= t_1$, too. This is not so correct from a physical description of microalgae and cyanobacteria growth, thus, algae growth was set to 0 until the latency time was reached. The second conditions stated that, once the latency time is over, the model should be then a monotonically not decreasing function, otherwise it was constantly equal to 0.

5.2.2 Dataset definition, variables domain and analysis of the experimental evidences

For the experimental dataset based on fired brick substrates, no novel experimental tests are performed, but a very large dataset coming from a previous work is used [25].
The adopted test apparatus is set according to previous works involving algae biofouling on building materials [15,25,27,28]. In particular, accelerated growth tests are performed in order to limit and avoid some methodological problems concerning its occurrence as readily observable and quantifiable phenomenon: if not accelerated, a visible biological deterioration usually starts after 1-year or more of natural exposure [14,115,116]. Concerning the microbial cultures chosen for the experimental tests, they are a green alga (*Chlorella mirabilis*) and a cyanobacterium (*Chroococcidiopsis fissurarum*), since they can be commonly found on building façades [61,66].
The different types of fired bricks are selected, and they have been cut into three prismatic samples with dimension equal to 8×8×3 cm3. To evaluate the effect of the substrate, the clay brick and stone materials selected for the experimental investigations are preliminarily characterized before the tests [15,25,32]. Total porosity P [-] of each material is determined

onto 3 samples by a mercury intrusion porosimeter (Micromeritics Autopore III) following the ASTM D4404-10 standard [117]. The surface roughness, as arithmetical mean roughness Ra [µm], is calculated according to UNI EN ISO 4287:2009 standard [118] and measured by using a Taylor Hobson CCI 3D Optical Profiler. The arithmetical mean deviation of the assessed profile is calculated on five sampling lengths of 5,54 mm.

For the environmental conditions with constant relative humidity, three different relative humidity conditions are reproduced inside three separate climatic chambers. The air of the indoor environment is conditioned by using different saturated solutions, following the methodology of reported in EN ISO 12571:2013 [119]. The RH equal to 75% is obtained through a saturated solution of NaCl, the RH at 87% through a saturated solution of Na2CO3, and the almost saturated relative humidity (98%) through only deionized water [120]. At the beginning of each test, samples are inoculated on 9 different points on their surface with the mixed culture per point. After the initial inoculation, samples are placed inside the climatic chambers and to exclusively evaluate the effect of relative humidity, during all the tests temperature is constantly controlled and maintained at 27.5 [25].

The investigations on the effect of temperature on algae growth follow the methodology adopted in previous researches since such methods well simulates the behavior of wall surfaces exposed to ''bad weather'', or leaky parts of a building or design defects [15,16,25,27,32,110]. It consists in accelerated tests with periodical water spray on the material surface: the algae suspension is sprinkled on sample surfaces, falling down their entire surface with run/off cycles of 15 minutes, for a total duration of 6 hours per day. In these experiments, relative humidity is assumed equal to 100%, since the wet&dry cycles allow to keep the sample surface wet during the test time. Tests are performed until the biofouling on each sample reached the stagnation phase at the end of the growth process. Figure 5.1 illustrates the scheme of the two apparatuses adopted in the accelerated growth tests under both constant temperature and relative humidity [25].
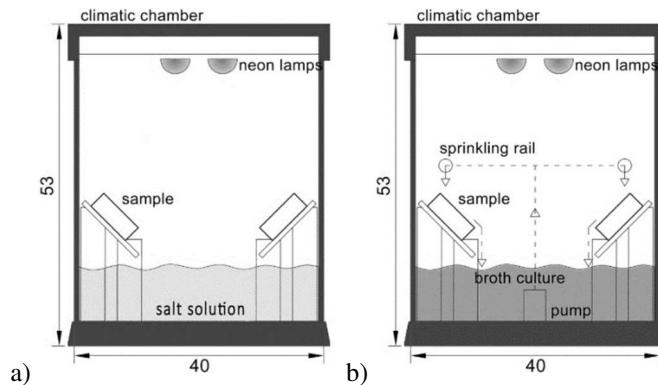
Figure 5.1. Scheme for the accelerated growth test apparatus adopted for the literature dataset [25]: a) under constant relative humidity conditions; b) under constant temperature conditions.

All the three growth chambers are placed in a dark room to avoid the influence of the external environment (daily light, outdoor temperature and relative humidity). Each test apparatus is

22

equipped with two neon lamps (Sylvania TopLife 39W) to provide an adequate illumination to simulate a day/night cycles of 14/10 h [25]. To monitor the environmental conditions set inside each growth chamber during the tests, temperature and humidity Sensirion SHT31-D sensors (https://www.adafruit.com/product/2857 , last access: December 2020) were connected to a National Instruments (NI) myRIO-1900 data logger device (https://www.ni.com/en-us/support/model.myrio-1900.html , last access: December 2020). Thanks to the small dimensions of the sensors (12,5 x 18 x 2,6 mm) it is possible to locate them near the samples. Such monitoring system has been previously tested and calibrated in other researches, aimed to characterize building materials and the surrounding environmental conditions investigate the critical conditions in terms of high moisture loads in the environment, i.e. of a hypogeum environment [121–126].

The dataset from [25] is chosen since it is (1) comparable to other dataset of previous failure model used in literature [7,29,37,108,109] and (2) representative of the most common influencing factor for algae growth, according to Section 5.2.1. Five different types of fired brick (SP_1, …, SP_5), having different porosity and roughness, are considered (Table 5.1), with three specimens for each type of brick, under seven different combinations of environmental conditions (EC_1, …, EC_7). Materials SP_1, SP_3 and SP_5 are considered for the empirical fitting process since they are comprehensive of the substrate domain (see condition(13)), representing the minimum, maximum and middle values for both porosity and roughness. SP_2 and SP_4 are used in the post fitting process in order to confirm its results because they are characterized by intermediate values of P and R. All the environmental conditions are taken into account in the fitting process. Hence, the dataset for the experimental fitting process is composed by 63 experimental algae growth curves, referring to 3 samples for 3 substrates under 7 different environmental conditions and by 56 curves for the confirmation step.

Substrate Properties			Environmental Conditions						
			Temperature [°C] – Relative humidity [%]						
	P [-]	R [μm]	EC_1	EC_2	EC_3	EC_4	EC_5	EC_6	EC_7
SP_1	0.19	4.50							
SP_2	0.19	5.54							
SP_3	0.25	2.95	T=27.5 RH=75	T=27.5 RH=87	T=27.5 RH=98	T=5 RH≈100	T=10 RH≈100	T=27.5°C RH≈100	T=40 RH≈100
SP_4	0.44	6.60							
SP_5	0.44	7.60							

Table 5.1. Tested surface properties (SP) and environmental conditions (EC) [25]. Three samples were tested for each surface property (SP).

An investigation of literature fired bricks surface properties is run [11,13,15,16,21,22,27,110–114] to see how the experimental data set (Table 5.1) fits with the literature and to set a general application range of the fired brick properties (i.e. porosity and roughness) for the empirical failure model. The review describes 60 different brick porosity values and 20 values of roughness (Figure 5.2). Moreover, the open porosity [%] considered in this work has been determined by a mercury intrusion porosimeter according

to the ASTM D4404-10 standard [117], and the surface roughness [μm] has been determined according to UNI EN ISO 4287:2009 standard [118], being the most commonly values in literature [13,16,21,27,110,114,127].

a)

b)
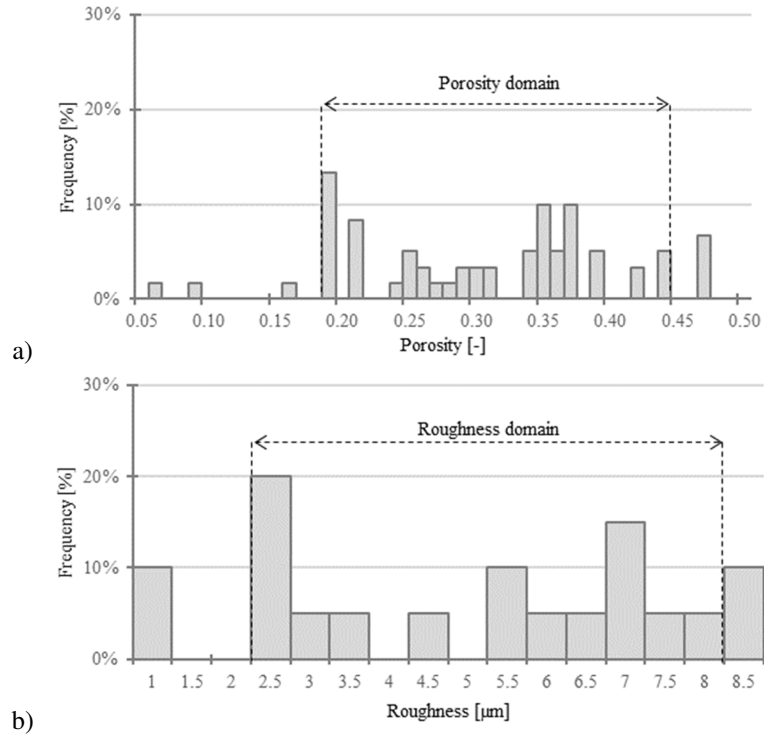
Figure 5.2. Comparison between porosity and roughness values from literature [11,13,15,16,21,22,27,110–114] and the porosity and roughness domain.

The domain for porosity P [-] and roughness R [μm] is set as reported in (13) by comparing the literature review results (Figure 5.2) [11,13,15,16,21,22,27,110–114] and the range of porosity and roughness from the experimental dataset chosen for the fitting process of the model (Table 5.1). In particular, it can be noted that the porosity domain set for the model is including 87% samples' values, while the roughness domain covers 80% of samples provided by literature. Calculation with values out of this domain has not granted results.

$$\begin{cases} 0.19 \le P \le 0.44 \\ 2.50 \mu m \le R \le 8.00 \mu m \end{cases} \tag{13}$$

Regarding the effect of the environmental conditions, it has been previously demonstrated that algae and cyanobacteria growth occurred only at saturation conditions, that is when free water is present. If no free water is available, algae growth does not happen. For taking into account such issue, from an engineering standpoint, a relative humidity $\ge 98\%$ is assumed as

a safety limit [25] even though brick surface could not be wet and water availability is only present by capillary condensation [128], by also considering that the approximation of the water activity with the relative humidity has already been demonstrated as acceptable [108]. Meanwhile, considering the temperature effect, algae biofouling occurs only for a limited range of temperature (between about 5°C and 40°C) [20,25,77]. Out of this range, it does not happen. Besides, it has an optimal temperature of growing (about 27.5°C), where the maximum coverage can be reached. The temperature T [°C] and relative humidity RH [%] domain set for the failure model is shown in (14) and, for T and RH values out of that, the algae growth is set equal to 0.

$$\begin{cases} 5°C \leq T \leq 40°C \\ RH \geq 98\% \end{cases} \tag{14}$$

Figure 5.3 shows the experimental trend of the parameter A_C/A_T, K and t_1 obtained by the literature results [25]: the parameters A_C/A_T and t_1 are determined directly from the measured data of each sample. On the other hand, K is calculated through iterations by minimizing the least squares value between experimental data and calculated values. The parameter values refer to the 3 specimens of the tested materials (SP$_1$, SP$_3$ and SP$_5$) under the environmental conditions RH>98% (EC$_4$, …, EC$_7$), for a total of 36 experimental data for each parameter. Since literature has shown that relative humidity determines the actual possibility for algae to growth, according to which growth happens only under $RH \geq 98\%$ [25], temperature effect can be separated from relative humidity and then analyzed. On the other hand, porosity and roughness have a combined effect on algae growth [16,25], hence, they are combined, even though they are still considered as separated variables.
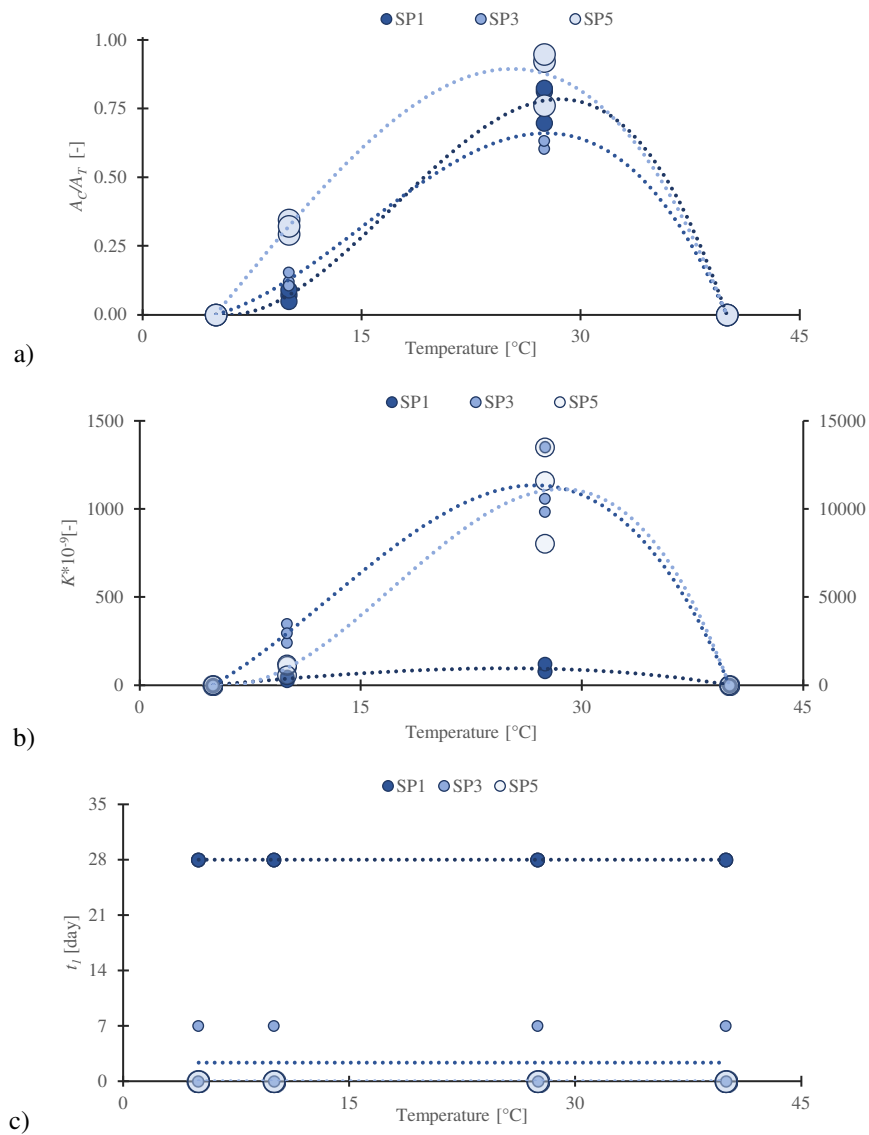
Figure 5.3. Experimental trend of bricks parameters: (a) A_C/A_T parameter; (b) K parameter; (c) t_1 parameter. The graphs are reported according to the temperature domain. The grey scale (light-dark) indicates the increasing porosity; the increasing dimension of the spot indicates the increasing roughness value. In (b) two y-axis were used since the K parameters are significantly different: SP_1 and SP_3 refer to the principal y-axis, SP5 refers to the 2nd y-axis.

According to Figure 5.3, it is evident that the environmental conditions primary affects the algae growth determining the actual possibility whether to start or not the process. In particular, relative humidity can be considered as an *on/off* factor, according to which algae growth is "on" for $RH \geq 98\%$. The temperature, in its domain, predominantly influences A_C/A_T and K parameters, determining an increasing trend from 5°C to 10°C, a more rapidly increasing trend between 10°C and 27.5°C and a decreasing trend from 27.5°C to 40°.For $T=5°C$ and $T=40°C$ both the covered area ratio and the growth rate parameters are null, and no signs of growth are detectable. Moreover, Figure 5.3 (a) and (b) highlights that porosity and roughness have a secondary effect on the A_C/A_T and K trends causing small variations on the cubic trend of determined by temperature according to the P and R values of the materials of SP_1, SP_3 and SP_5. In this way, aiming at determining the simplest possible model, having only 4 different temperature values, a 3rd degree polynomial was set in order to describe A_C/A_T and K as functions of T, having its coefficients depending on P and R. Lastly, in Figure 5.3 (c) the latency time t_1 shows a constant trend not depending on temperature, conversely, it is strongly influenced by the substrate.

Hence, these experimental evidences can be converted into equations as in condition (15):

$$\begin{cases} \Omega(RH) = \begin{cases} 0, & RH < 98\% \\ 1, & RH \geq 98\% \end{cases} \\[2mm] \dfrac{A_C}{A_T}(T,P,R) = a_3(P,R) \cdot T^3 + a_2(P,R) \cdot T^2 + a_1(P,R) \cdot T + a_0(P,R) \\[2mm] K(T,P,R) = b_3(P,R) \cdot T^3 + b_2(P,R) \cdot T^2 + b_1(P,R) \cdot T + b_0(P,R) \\[2mm] t_1(P,R) = c_0(P,R) \end{cases} \quad (15)$$

where $a_{3,P,R}, \ldots, a_{0,P,R}, b_{3,P,R}, \ldots, b_{0,P,R}$ and $c_{0,P,R}$ are the temperature coefficients respectively for the A_C/A_T, K and t_1 parameters. From the above, these coefficients are set as function of porosity and roughness. The equation of the $a_{n,P,R}$, $b_{n,P,R}$ and $c_{0,P,R}$ resulted from the fitting process (see Section 5.2.3).

Moreover, form the experimental evidence in Figure 5.3 it is possible to define the codomain of the covered area by algae growth and its relative parameters as reported in equation (16):

$$\begin{cases} 0 \leq X(t,T,RH,P,R) \leq 1 \\[2mm] 0 \leq \dfrac{A_C}{A_T}(T,P,R) \leq 1 \\[2mm] K(T,P,R) \geq 0 \\[2mm] t_1(P,R) \geq 0 \end{cases} , \forall T \in [5;40], \forall RH \in [0;100], \forall P \in [0.19;0.44], \forall R \in [2.50;8.00] \quad (16)$$

5.2.3 Fitting and validation processes

For the fitting process data from materials SP_1, SP_3 and SP_5 are considered since they are comprehensive of the substrate domain (see Section 5.2.2), representing the minimum, maximum and middle values for both porosity and roughness. On the other hand, SP_2 and SP_4 are used in the post fitting process in order to confirm its results since they are characterized by intermediate values of P and R. All the environmental conditions are taken into account in the fitting process.

The goal of the fitting process is to determine the equations based on fired bricks surface properties (P [-] and R [μm]) and respectively their coefficient that result in the $a_{n,P,R}$, $b_{n,P,R}$ and $c_{0,P,R}$ temperature coefficients.

The $a_{n,P,R}$ and $b_{n,P,R}$ and $c_{0,P,R}$ coefficients are written as a n-grade polynomial function of P and R, following the equations in (17):

$$\begin{cases} a_n(P,R) = \sum_{j=0}^{n} \alpha_{j,a_n} P^j + \sum_{k=0}^{n} \beta_{k,a_n} R^k \\[2mm] b_n(P,R) = \sum_{j=0}^{n} \alpha_{j,b_n} P^j + \sum_{k=0}^{n} \beta_{k,b_n} R^k \\[2mm] c_0(P,R) = \sum_{j=0}^{n} \alpha_{j,c_0} P^j + \sum_{k=0}^{n} \beta_{k,c_0} R^k \end{cases} \quad (17)$$

where α_j, and β_k, are the resulting coefficients. The fitting process is iterative: it starts considering grade 0 for both P and R and it continues by alternatively and then jointly increasing the degree of P and R. Nevertheless, no more than 3 terms for each polynomial equation of $a_{n,P,R}$, $b_{n,P,R}$ and $c_{0,P,R}$ can be defined, having only three considered materials (SP_1, SP_3 and SP_5). They might be be different for each temperature coefficients.

The process stops when the following two requirements are achieved. The first requirement verifies the analytical correctness of the model by determining the adjusted coefficient of determination R^2_{adj} since a multiple variable regression has been considered. The calculation of R^2_{adj} is shown in equation (18) and all the R^2_{adj} have to be higher than 0.85 [89].

$$R^2_{adj} = 1 - \frac{RSS}{TSS} \cdot \frac{n-1}{n-p-1} \geq 0.85 \quad (18)$$

The *RSS* is the residual sum of squares between the experimental and the fitted data, *TSS* is the total sum of squares of the differences between the experimental data and its mean, n is the number of observation and p is the total number of explanatory variables in the model [129]. The coefficients R^2_{adj} are determined considering the A_C/A_T and K and t_1 fitted parameters and the respective experimental ones determining the general fitting quality of the model.

Subsequently, the second requirement involves the experimental correctness of the model. It is satisfied when condition (19) is fulfilled.

$$\begin{cases} \min\left[\dfrac{A_C}{A_T}_{\text{exp}}\right] \leq \dfrac{A_C}{A_T}(T,P,R) \leq \max\left[\dfrac{A_C}{A_T}_{\text{exp}}\right] \\[4mm] \min\left[K_{\text{exp}}\right] \leq K(T,P,R) \leq \max\left[K_{\text{exp}}\right] \\[4mm] \min\left[t_{1,\text{exp}}\right] \leq t_1(P,R) \leq \max\left[t_{1,\text{exp}}\right] \end{cases} \qquad (19)$$

Whether such requirements are not fulfilled, the iterative fitting process is started over.
The validation process considers the surface properties of SP$_2$ and SP$_4$ materials. The methods used for the validation process are the same. Firstly, the R$^2_{\text{adj}}$ is determined for the three parameters A_C/A_T, K and t_1 of such materials and they still have to be higher than 0.85, as analytical requirement. Then, the experimental correctness is verified by condition (19).

5.3 The dynamic model

5.3.1 Basic assumptions

The basic assumptions of the dynamic model are made to guarantee the correctness and reliability of the growth curves even in variable environmental conditions. It also has to ensure an easy implementation of the model on simulation software, especially according to the outputs that they obtain, often written as a time history of temperature and relative humidity. Furthermore, since the static version model remains by forming the theoretical basis for the dynamic version, the assumptions, theories and hypotheses expressed so far are only analytically rewritten and adapted to the process of calculating the dynamic curve.
The first assumption concerns time by stating that time is no longer a continuous variable, but it is discretized in daily intervals. The measurement of this interval is daily and it is taken in accordance with the unit of measurement expressed for t_1 and with the experimental measurement mode [15,25,27,28,32]. With the appropriate modifications, however, it can be reduced in hours. This assumption allows to dialogue with the software outputs such as the time histories of T and RH [39–41]. In accordance with this assumption, it can be therefore assumed that $T(t)$ and $RH(t)$ are constant for each time interval. On the contrary, the conditions of the substrate do not change over time, as already established by the previous failure model and also reported among the requirements of the static model [32].
The second and third basic assumptions arranges the development of algae growth over time and therefore with varying environmental conditions.
They state that the overall growth curve still remains increasing or at most constant over time, even when the $T(t)$ and $RH(t)$ change to a less favorable condition. Moreover, the effect of environmental conditions changes directly affects the overall growth rate, not the covered area; in fact, the covered area remains unaltered at the moment the change in temperature or relative humidity happens. This concept has been previously anticipated in [32] by the

conservation principle of the reached covered area and the curves combination through a horizontal asymptote. The combination method is shown in Figure 5.4. At the moment the temperature T_i changes, the horizontal asymptote corresponding to the reached covered area is depicted. It crosses the curve of the T'_{i+1} but not the one of T''_{i+1}: that means that, for T'_{i+1}, algae can keep growing, since they have not already reached the relative maximum covered area, hence the growth rate can be still increasing; for the T''_{i+1} curve, algae cannot growth further, having already reached the relative maximum covered area, hence the overall rate is kept constant. Figure 5.4 (b) shows the combination results.
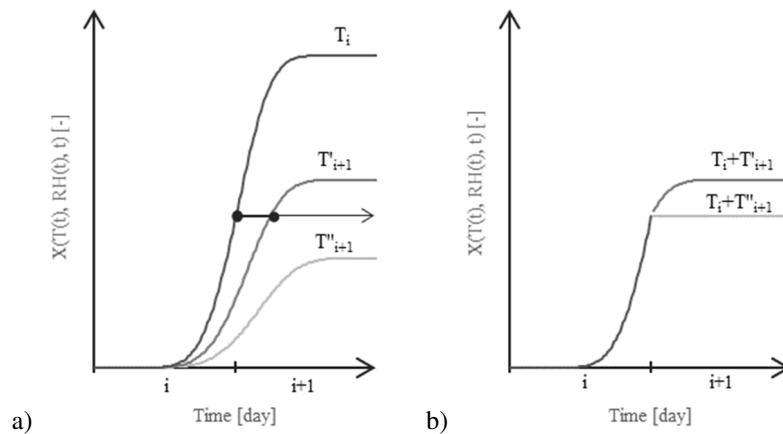
Figure 5.4. Examples of overall growth curve under dynamic temperature $T(t)$:
a) combination method; b) results

5.3.2 The calculation process

The calculation process of the dynamic model involves three parts: the first part regards the setting of the model time, the second involves the definition of the variable for each time interval, while the third explains the steps aimed at the determination of the growth overall process.

The definition of the model time is a primary step since the growth time and the running time of the simulation could differ from each other. The simulation time s_t corresponds to the entire simulation time, that is the time of the temperature and relative humidity file history. It consists in a list of $T(s_t)$ and $RH(s_t)$ values, usually daily or hourly [39–41]. In this work, the start of growth time g_t, on the other hand, is set only when a combination of $T(s_t)$ and $RH(s_t)$ can activate the algae growth. According to literature evidence and to the domains of T and RH, this combination is (20)

$$\begin{cases} 5°C \leq T(t_s) \leq 40°C \\ RH(t_s) \geq 98\% \end{cases}$$ (20)

30

Hence, at the first i-th value of simulation time that validates condition (20) the growth time g_t starts running, as shown in Figure 5.5. For sake of simplicity, from now on the growth time g_t is indicated as time t [day].
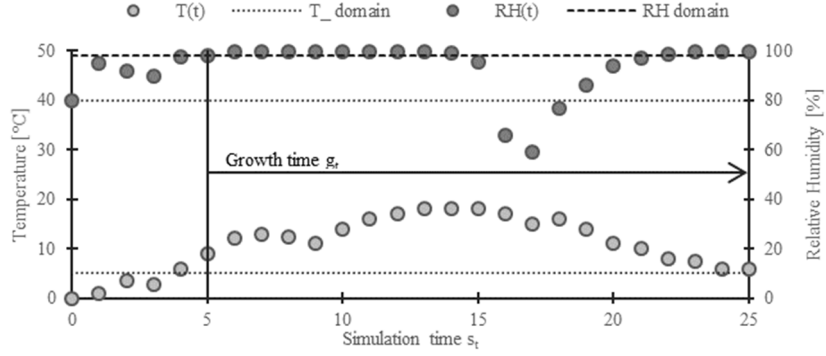
Figure 5.5. Determination of the growth time t_g compared to the simulation time t_s: example.

Regarding the setting of the variable, as stated in the dynamic model requirements (Section 5.3.1), P and R are assumed constant over the time, while $T(t)$ and $RH(t)$ are specific and constant for each time interval. Knowing that, all the model parameters A_C/A_T $(T(t), P, R)$, K $(T(t), P, R)$ and t_1 (P) can be defined for each i-th time interval (Table 5.2).

Time interval t	t_{i-1}	t_i	t_{i+1}
Variables	T_{i-1}	T_i	T_{i+1}
	RH_{i-1}	RH_i	RH_{i+1}
	P	P	P
	R	R	R
Parameters	A_C/A_T (T_{i-1}, P, R)	A_C/A_T (T_i, P, R)	A_C/A_T (T_{i+1}, P, R)
	K (T_{i-1}, P, R)	K (T_i, P, R)	K (T_{i+1}, P, R)
	t_1 (P, R)	t_1 (P, R)	t_1 (P, R)
Output	X_{i-1}	X_i	X_{i+1}

Table 5.2. Definition of variables, parameters and output according to the time interval.

Lastly, since the latency time t_1 (P, R) is not varying over time according to Table 5.2, due to its only dependence on porosity and roughness, the condition (12) of the static failure model (Section 5.2.1) is applied to the dynamic model as reported in (21).

$$X_i = 0, \ \forall t_i < t_1(P, R) \tag{21}$$

The third part of this section involves the determination of the overall growth curve. Having assumed the graphical method of the horizontal asymptote [32], the combination of the curves can be analytically determined by the time shift $t_{s,i}$ definition. This allows to have the same reached covered area X_i and $X(Tt_{i+1}, t_i)$ in the same instant of time i, with the temperature varying between T_i and T_{i+1} as shown in Figure 5.6.
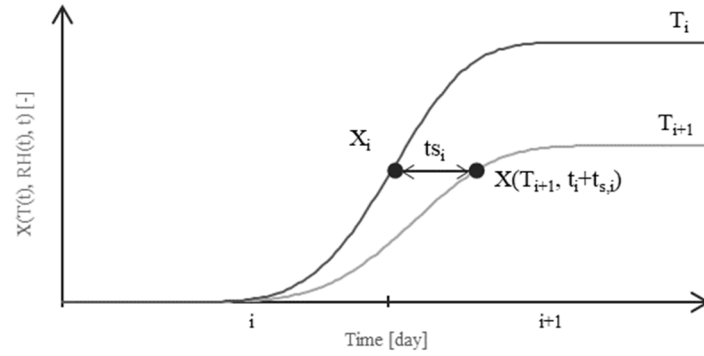
Figure 5.6. Graphical explanation of the time shift $t_{s,i}$ definition.

The analytical definition of the time shift $t_{s,i}$ [day] is hence presented in condition (22):

$$t_{s,i} = \sqrt[4]{-\left(\frac{1}{K(T_{i+1})}\right) \cdot \ln\left(1 - \frac{X_i}{\frac{A_C}{A_T}(T_{i+1})}\right)} - t_i + t_1 \tag{22}$$

The 4th root result is assumed positive since the time can't be negative. Moreover, X_i is always higher than A_C/A_T (T_{i+1}) according to the basic assumption in Section 5.3.1.

32

Chapter 6

Toward a new theory for algae growth: the logistic function

This chapter deepens the second goal of this novel approach: the identification of a new basic theory that can describe algae growth and overcome Avrami's flaws.

As previously presented in this work (Section 3.1), the Avrami's theory has some limitation in correctly predicting the algae growth. The first limitation involves a very fast growth that escape the latency phase, while, the second one is an analytical bug that causes a small decreasing trend at the growth start. Both of the flaws are not recurrent, and they can be even dismissed, but they are not correct from a physical point of view. On the other hand, its application is extended to different type of porous building materials (e.g. bricks, sandstone and limestone) under different environmental temperature and relative humidity and even considering the effect of surface treatments.

Consequently, this work compares this latter theory with the logistic formula, identified by numerous studies as adequate to describe the growth of a population, from virus, to microorganisms up to human (see Section 3.2). Firstly, the experimental dataset previously analyzed by the Avrami's theory is collect, considering also the relative influencing factors for the algae growth such as porosity, roughness, temperature and surface treatments (see Section 6.1). Then, the logistic model is applied to such dataset and the comparison of the two models is run verifying if the logistic model:
- can better overlap the experimental data (Section 6.2.1);
- can overcome the Avrami's flaws (Section 6.2.2);
- is less influenced by the algae growth influencing factors (Section 6.2.3).

6.1   Experimental dataset definition

In order to have a wide comparison between the logistic formulation and the Avrami's theory, all the literature concerning algae growth on building materials and its modelling with the Avrami's theory are analyzed [15,25,27,28]. Although the core of this work concerns fired brick surfaces, stones are also considered within this section aiming to determine an approach that will concern in the future all porous and not porous building materials. Such data involved two more material type, other than brick (i.e. brick, limestone and sandstone), different substrate properties (in terms of porosity P [-] and roughness R [μm]), two growth temperature T [°C] and biocides surfaces treatment. Since microalgae growth curves are strongly influenced by substrate properties, such as porosity and roughness, environmental conditions and eventual surface treatments, such factors are also considered for the models' accuracy.

Table 6.1 shows the substrate properties, environmental temperature and biocides for brick type material selected from literature [15,25,27].

Substrate Properties					Environmental Conditions		Surface Treatment	
Type	Ref	Name	P [-]	R [µm]	T= 10°C	T= 27.5°C	No	Yes - Type
Brick	[27]	LSU	0.19	2.4		✓	✓	
		LST	0.19	2.4		✓		TiO$_2$
		LRU	0.19	2.8		✓	✓	
		LRT	0.19	2.8		✓		TiO$_2$
	[15]	NNt	0.19	2.8		✓	✓	
		NAg	0.19	2.8		✓		TiO$_2$+Ag
		NCu	0.19	2.8		✓		TiO$_2$+Cu
	[25]	AS	0.19	4.5	✓		✓	
		AS	0.19	4.5		✓	✓	
		AR	0.19	5.54	✓		✓	
		AR	0.19	5.54		✓	✓	
		B	0.25	2.95	✓		✓	
		B	0.25	2.95		✓	✓	
	[27]	HSU	0.37	1.1		✓	✓	
		HST	0.37	1.1		✓		TiO$_2$
		HRU	0.37	8.9		✓	✓	
		HRT	0.37	8.9		✓		TiO$_2$
	[15]	ANt	0.37	8.9		✓	✓	
		AAg	0.37	8.9		✓		TiO$_2$+Ag
		ACu	0.37	8.9		✓		TiO$_2$+Cu
	[25]	CS	0.44	6.6	✓		✓	
		CS	0.44	6.6		✓	✓	
		CR	0.44	7.6	✓		✓	
		CR	0.44	7.6		✓	✓	

Table 6.1. List of the porous building materials considering substrate properties, environmental conditions and surface treatments for fired brick surfaces [15,25,27].

Table 6.2 shows the substrate properties, environmental temperature and biocides for stone type material (sandstone and limestone) selected from literature [28].

					Environmental Conditions		Surface Treatment	
Substrate Properties								
Type	Ref	Name	P [-]	R [µm]	T= 10°C	T= 27.5°C	No	Yes - Type
Sandstone	[28]	A2	0.05	7.9		✓	✓	
		A2T	0.05	7.9		✓		TiO2
		A1	0.08	7.6		✓	✓	
		A1T	0.08	7.6		✓		TiO2
Limestone	[28]	C3	0.08	2		✓	✓	
		C3T	0.08	2		✓		TiO2
		C1	0.09	2.6		✓	✓	
		C1T	0.09	2.6		✓		TiO2
		C2	0.18	2.6		✓	✓	
		C2T	0.18	2.6		✓		TiO2

Table 6.2. List of the porous building materials considering substrate properties, environmental conditions and surface treatments for stones [28].

All the Avrami's curves and the relative parameters A_C/A_T, K and t_1 are thus collected. Even if the Avrami's model fails in overlapping the experimental data, as reported by the authors [15], the ANt, AAg and ACu curves are reported for a better clarity and completeness of the comparison.

6.2 Comparing the Avrami's theory and the logistic equation: methods

6.2.1 Overlapping the experimental data

The first comparison involves the assessment of which model could better overlap the experimental data. To assess that, the comparison is run evaluating: (1) how many times the model overlaps the data and their fitting quality. Concerning the values out per each model, this work evaluates when they are out according to each growth phase and how far from the experimental data they are.

For the first comparison, this works determines the percentage of values that validates condition (23):

$$\min(X_{\exp_1},...,X_{\exp_3})_i \le X(t=i) \le \max(X_{\exp_1},...,X_{\exp_3})_i \tag{23}$$

where $X(t=i)$ is the calculated covered area for both the models at the i-th time of the measure and $X_{exp1}, ..., X_{exp3}$ correspond to the experimental measures of the 3 samples respectively.
To the same aim, a comparison between the fitting quality index $R_\%$ [-] of the two models is run. This index was previously adopted for the Avrami's law [25–28], and it was calculated according to equation (24):

$$R_\% = \sqrt{\frac{\sum\limits_{t=i}\left(X(t=i)-X_{\exp_{m,i}}\right)^2}{\sum\limits_{t=i}X_{\exp_{m,i}}}} \cdot 100 \tag{24}$$

where $X(t=i)$ and $X_{\exp m,i}$ represent the calculated and the average experimental data at time $t=i$, respectively. This value expresses the deviation between experimental data and simulated one, that is, the more it tends to zero, the more the analytical model overlaps the measured data.
For the second step, the discretization of the average experimental data into the three phases is run according these steps:
- the total slope of the experimental data m_{tot} is determined considering the starting point, that corresponded to the covered area at time 0, and the ending point, where both the time and the microalgae coverage are at their maximum;
- the i-th slope m_i is determined between the covered area at time i and the previous measure at time $i-1$;
- the three phases are evaluated according to condition (25)

$$\begin{cases} \text{Exponential} & m_i > m_{tot} \\ \text{Latency, Stagnation} & m_i \le m_{tot} \end{cases} \tag{25}$$

This discretization method defines the exponential phase as the phase in which the growth slope m_i is higher than the linear growth in the total period of growth (m_{tot}); conversely, both the latency and stagnation take place when m_i is equal or lower than m_{tot}, respectively, right before and after the exponential phase. Figure 6.1 shows an example of such discretization: the first 11 experimental data and the last 7 values are grouped respectively in the latency/stagnation phase, since their m_i values are always lower than m_{tot}; conversely, the remaining experimental values can be grouped in the exponential phase because their m_i are higher than the m_{tot}.
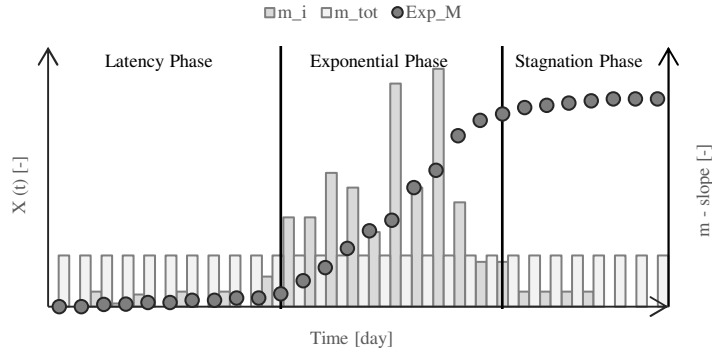
Figure 6.1. Example of average experimental data discretization into the latency/exponential/stagnation phase. Black dots represent the average experimental data; vertical bars represent the m values, respectively grey for the i-th value and white for the total. The 2nd axis was used for the m values.

Hence, for each growth phase Gp, the percentage of the values resulting out of the experimental range is analyzed according to (26)

$$\left(\frac{number\ of\ X_{out}}{number\ of\ X_{tot}} \right)_{Gp} \tag{26}$$

comparing the number of times values are out (X_{out}) to the number of total values (X_{tot}).
The goal of the last comparison is to evaluate eventual trend of under/over estimation for such out values and, thus, to asses if one of the models is closer to the experimental data, even when not properly overlapping the data. For every i-th out values, the underestimation/overestimation is calculated by determining the difference between the calculated $X(t=i)$ and the minimum/maximum experimental value among the three sample $(X_{exp1}, \ldots, X_{exp3})_i$ according to (27):

$$\begin{cases} \dfrac{X(t=i) - \min(X_{exp_1}, ..., X_{exp_3})_i}{\dfrac{A_C}{A_T}} & \text{if } X(t=i) < \min(X_{exp_1}, ..., X_{exp_3})_i \\[4em] \dfrac{X(t=i) - \max(X_{exp_1}, ..., X_{exp_3})_i}{\dfrac{A_C}{A_T}} & \text{if } X(t=i) > \max(X_{exp_1}, ..., X_{exp_3})_i \end{cases} \tag{27}$$

Moreover, a normalization of such differences to the total covered area A_c/A_t is run in order to have comparable results. In fact, the total covered area significantly differ among all the materials, ranging between 0.10 and 1.00 [15,25,27,28]. Since A_C/A_T is the same for both the formulations, results are not influenced. It is determined for both the models. Boxplot analysis is run to describe the trend and distribution of such values for each phase [125].

6.2.2 Overcoming the Avrami's flaw

The first step of this work part is to validate the hypothesis that the Avrami's model is not able to correctly simulate microalgae growth ANt, ACu and AAg because the latency phase is missing in such materials [15]. In order to verify that, all the materials resulting with no latency phase from the discretization above are collected. Subsequently, the work verifies whether the logistic equation is able to overcome such flaw by determining if the curve can simulate the growth without the latency phase, as for the experimental data. Moreover, even though this work has already proven that the logistic has an increasing trend for every time values, such flaw was graphically verified for all the materials with $t_1>0$.

6.2.3 Correlation with growth influencing factors

The third comparison is run to assess which model is less influenced by the microalgae influencing factors such as porosity and roughness, surface treatments, as well as different environmental conditions (temperature). To evaluate the correlation with each factor alone, three subsets are formed:
- Porosity and Roughness subset: with all the untreated material under T=27.5°C;
- Temperature subset: all the untreated material under T=10°C and T=27.5°C, respectively;
- Surface Treatment subset: all the treated and respectively untreated materials under T=27.5°C.

Three categories are correlated to each subset. The first one is the numbers of values inside the experimental range, the second one considers the values out according to each growth phase (latency, exponential and stagnation phase) and the third one involves the fitting quality index $R_{\%}$ [-]. The first two categories are set aiming at describing the effect of the influencing factors from the experimental side while the third one evaluates the correlation from the fitting quality side. The correlation for both models is assessed trough the coefficient of determination R^2 [-] [130]. In particular, the effect of porosity and roughness is considered as a combined effect through a fitting surface determined as a 1st degree polynomial equation determined on MATLAB R2017 software [131]. For temperature and surface treatments, a linear regression is considered. Since the second one is a binary regressor (untreated/ treated), binary indicator variables are used respectively 0 for the untreated materials and 1 for the treated ones [130]. The correlation is assessed when the determined R^2 was higher than 0.50 [130] and the obtained trend are evaluated through scatter plot.

Chapter 7

Results of the model development process

7.1 The ALGAE failure model equations

The final equation of the model is presented in (28)

$$X(RH_i, T_i, P, R, t_i) = \Omega(RH_i) \cdot \frac{A_C}{A_T}(T_i, P, R) \cdot \left(1 - \exp^{-K(T_i, P, R)\left(t - t_1(P, R) + t_{s,i}\right)^4}\right) \tag{28}$$

and it can both describe algae growth on fired bricks under both static and dynamic environmental conditions (RH_i, T_i). The parameters of the model are determined as the following condition (29), according to general requirements, experimental evidences and analytical findings.

$$
\begin{cases}
\Omega(RH_i) = \begin{cases} 0, & RH < 98\% \\ 1, & RH \geq 98\% \end{cases} \\[2em]
\frac{A_C}{A_T}(T_i, P, R) = a_{3,P,R}T_i^3 + a_{2,P,R}T_i^2 + a_{1,P,R}T_i + a_{0,P,R} \\[2em]
K(T_i, P, R) = b_{3,P}T_i^3 + b_{2,P}T_i^2 + b_{1,P}T_i + b_{0,P} \\[2em]
t_1(P, R) = c_{0,P} \\[2em]
t_{s,i} = \sqrt[4]{-\left(\frac{1}{K(T_{i+1})}\right) \cdot \ln\left(1 - \frac{X(t_i)}{\frac{A_C}{A_T}(T_{i+1})}\right)} - t_i + t_1
\end{cases}
\tag{29}
$$

The equations for $a_n (P,R)$, $b_n (P,R)$ and $c_0 (P)$ in function of porosity P [-] and roughness R [µm] resulting from the fitting process are showed in condition (30).

$$\begin{cases} a_n(P,R) = \alpha_{2,a_n} P^2 + \beta_{1,a_n} R + \beta_{2,a_n} R^2 \\[2mm] b_n(P) = \alpha_{1,b_n} P + \alpha_{3,b_n} P^3 + \dfrac{\beta_{8,b_n}}{R^8} \\[2mm] c_0(P) = \dfrac{\alpha_{8,c_0}}{P^8} + \beta_{1,c_0} R + \beta_{2,c_0} R^2 \end{cases} \qquad (30)$$

The solutions of the systems are uniquely determined, since 3 different coefficients result for each equation considering just 3 materials (i.e. SP_1, SP_3 and SP_5). All the units unit of measure and order of magnitude for P, R, T and RH are set according to the experimental dataset values (Table 5.1). Table 7.1 resumes such information and shows the $\alpha_j, ..., \beta_k$ values for all the coefficients.

Parameter	T-coeff	**Coefficients**						
		α_1	α_2	α_3	α_8	β_1	β_2	β_8
A_C/A_T	a_3	-	$5.0000*10^{-4}$	-	-	$-5.2100*10^{-5}$	$4.1980*10^{-6}$	-
	a_2	-	$-3.9800*10^{-2}$	-	-	$2.8023*10^{-3}$	$-2.1840*10^{-4}$	-
	a_1	-	$8.7980*10^{-1}$	-	-	$-3.1032*10^{-2}$	$2.1600*10^{-3}$	-
	a_0	-	-3.4190	-	-	$9.2000*10^{-2}$	$-5.7000*10^{-3}$	-
K	b_3	$7.709831*10^{-10}$	-	$-2.315303*10^{-8}$	-	-	-	$1.169671*10^{-7}$
	b_2	$-3.978387*10^{-8}$	-	$1.173803*10^{-6}$	-	-	-	$-1.081282*10^{-5}$
	b_1	$3.832828*10^{-7}$	-	$-1.056712*10^{-5}$	-	-	-	$2.729806*10^{-4}$
	b_0	$-1.018137*10^{-6}$	-	$2.638435*10^{-5}$	-	-	-	$-1.109344*10^{-3}$
t_1	c_0	-	-	-	$4.73*10^{-5}$	$-2.88*10^{-4}$	$-2.66*10^{-4}$	-

Table 7.1. Coefficients for fired bricks surfaces resulting from the fitting.

7.2 Result of fitting and validation processes

Concerning the general fitting quality between the fitted trend and the experimental ones, Figure 7.1 shows that the R^2_{adj} is always higher than 0.85 for all the three parameters. This means that the regression predictions fit the 63 datapoint of SP_1, SP_3 and SP_5, used to determine the model.

Figure 7.1. Coefficient of determination R^2_{adj} of the parameters. (a) A_C/A_T parameters; (b) K parameter; (c) t_1 parameter. The grey scale (dark-light) indicates the increasing porosity; the increasing dimension of the spot indicates the increasing roughness value. In (b) two y-axis were used since the K parameters are significantly different: SP_1 and SP_3 refer to the principal y-axis, SP_5 refers to the 2nd y-axis.

Lasty, both the experimental values (e.g. A_C/A_T, K and t_1) and the fitted curves (e.g. A_C/A_T (T,P,R), K (T,P) and t_1 (P)) for the three parameters are reported in Figure 7.2. As shown in Figure 7.2, the curves are falling within the experimental values, verifing the condition proposed in (19).
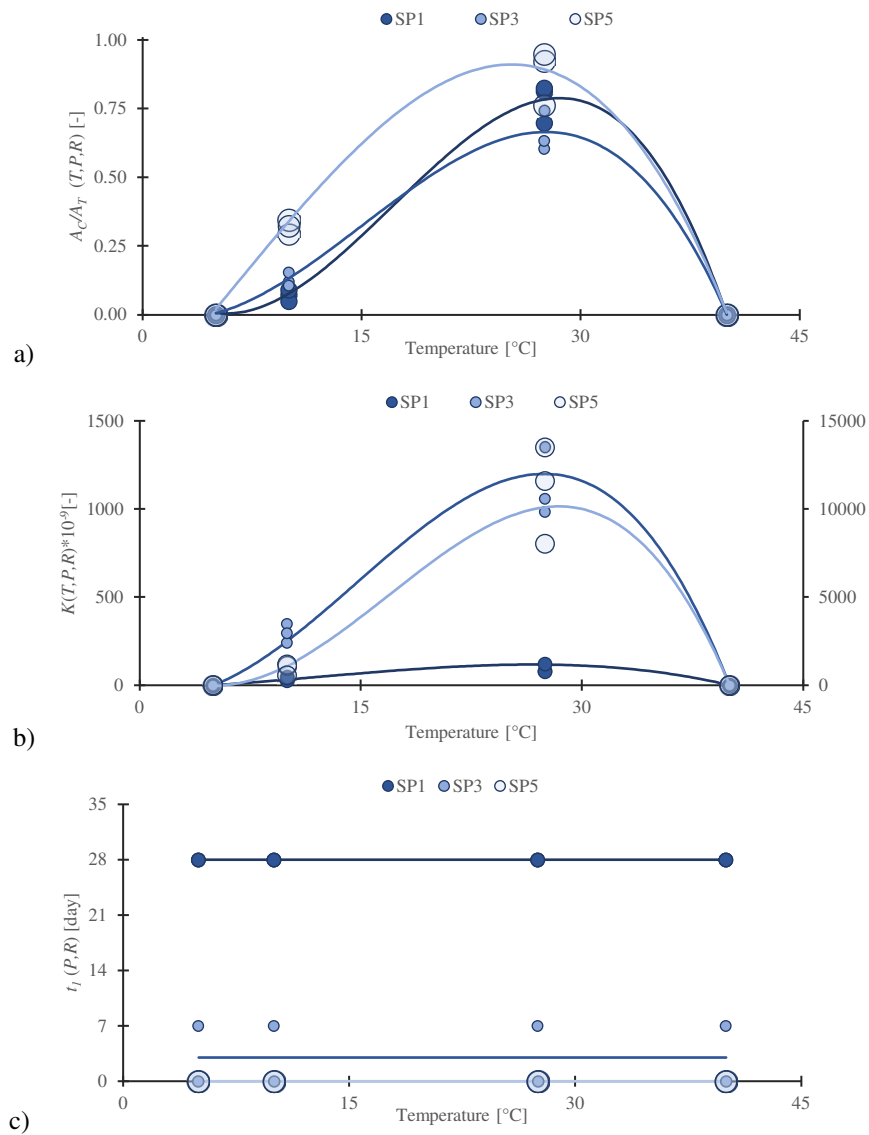
Figure 7.2. Comparison between the experimental values and the fitted curves for the surfaces properties SP_1 SP_3 and SP_5: (a) A_C/A_T (b) K and (c) t_1. The grey scale (dark-light) indicates the increasing porosity; the increasing dimension of the spot indicates the increasing roughness value. In (b) two y-axis were used since the K parameters are significantly different: SP_1 SP_3 refer to the principal y-axis, SP_5 refers to the 2nd y-axis.

As shown in Figure 7.3, R^2_{adj} is always higher than 0.85 for SP_2, and SP_4 used for the validation process.
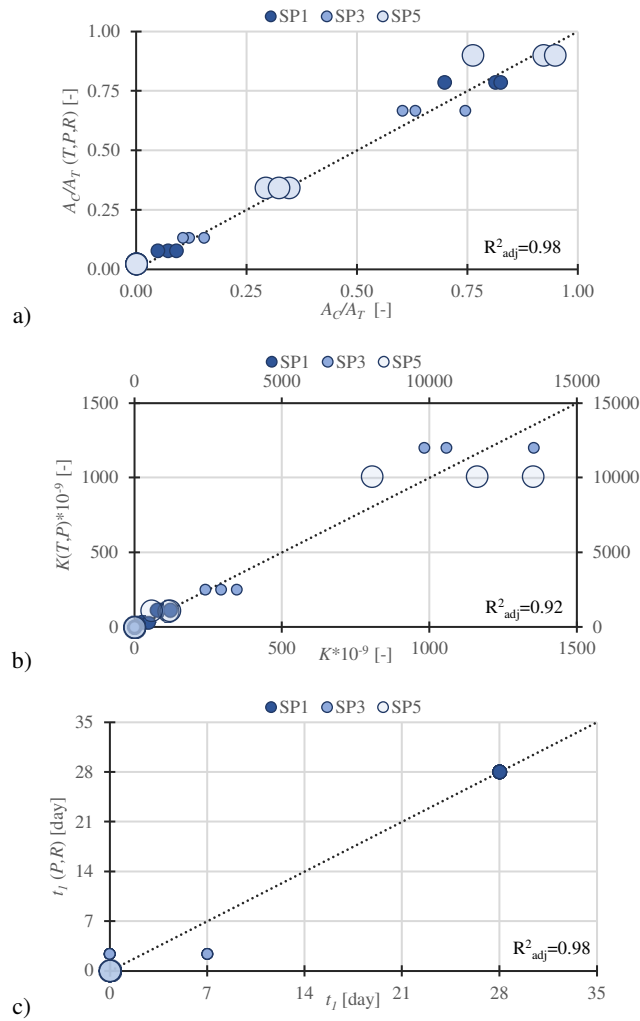
a)

b)

c)
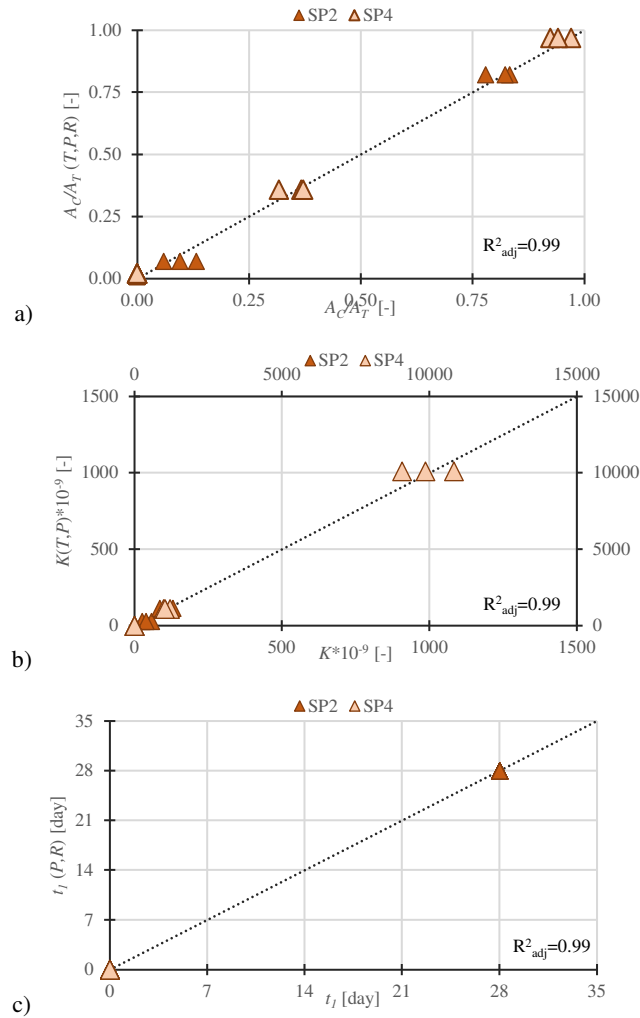
Figure 7.3. Coefficient of determination R^2_{adj} of the parameters. (a) A_C/A_T parameters; (b) K parameter; (c) t_1 parameter. The grey scale (dark-light) indicates the increasing porosity; the increasing dimension of the spot indicates the increasing roughness value. In (b) two y-axis were used since the K parameters are significantly different: SP_2 refer to the principal y-axis, SP_4 refers to the 2nd y-axis.

Figure 7.4 shows that the curves determined by the failure model fall within the range of their respective experimental data. The model is therefore validated for the surface properties SP_2, and SP_4.
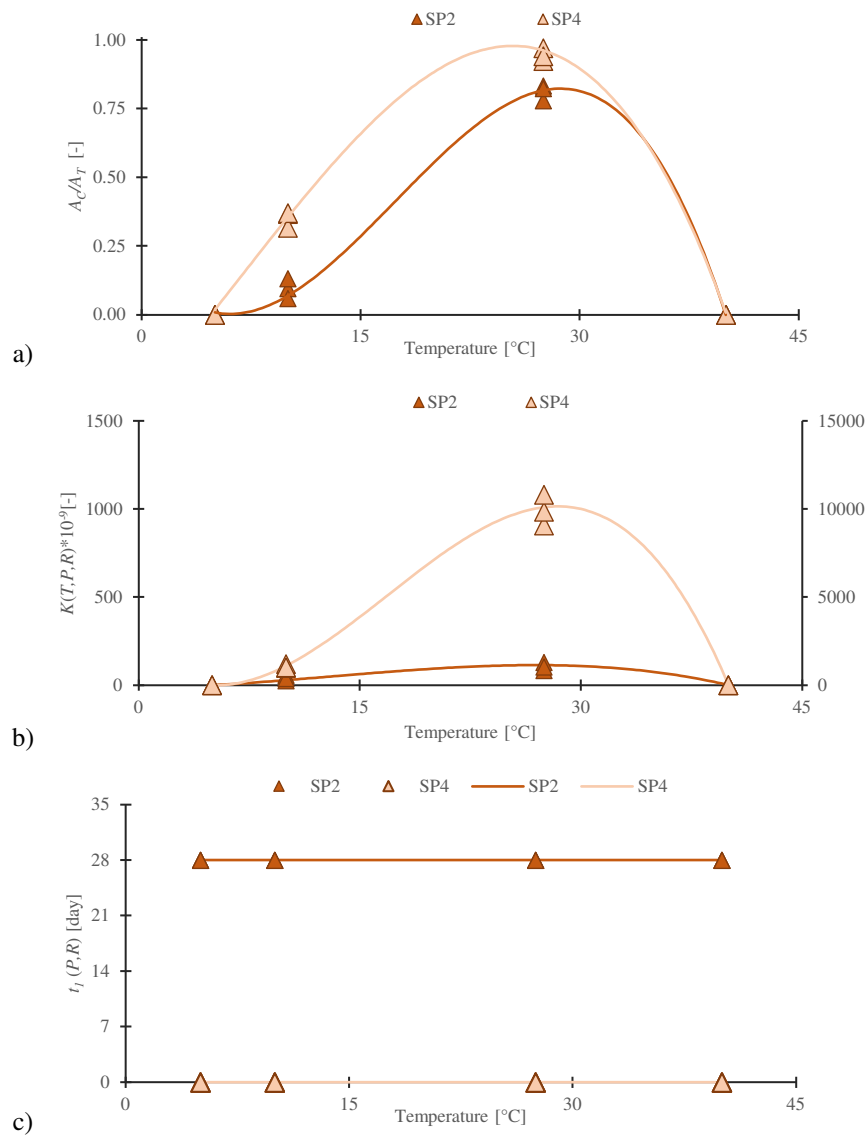
Figure 7.4. Comparison between the experimental values and the fitted curves for the surfaces properties SP$_2$ and SP$_4$: (a) A_C/A_T (b) K and (c) t_1. The grey scale (dark-light) indicates the increasing porosity; the increasing dimension of the spot indicates the increasing roughness value. In (b) two y-axis were used since the K parameters are significantly different: SP$_2$ refers to the principal y-axis, and SP$_4$ refers to the 2nd y-axis.

As a last qualitative validation step, according to other previous model validation [29,109], the curves describing microalgae growth X (t, T, RH, P, R) are determined for the validation

substrates SP$_2$ and SP$_4$ under the tested environmental condition EC$_5$ and EC$_6$ (Table 5.1) and overlap to the experimental data obtained in [25]. All the curves well fit the experimental values (Figure 7.5).
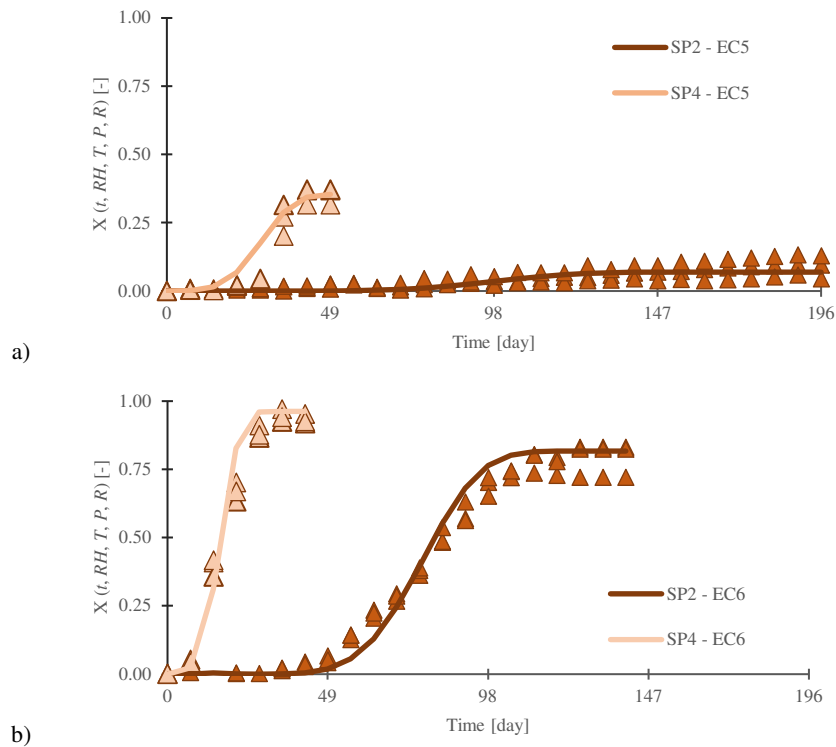
Figure 7.5. Comparison of the covered area $X(t, T, RH, P, R)$ obtained with the failure model and experimental data for SP$_2$, and SP$_4$ [25]:a) when exposed to EC$_5$;b) when exposed to EC$_6$. Lines indicate the failure model curves; points indicate the experimental data obtained in [25].

7.3 Application of ALGAE failure model

7.3.1   Application to different dynamic environmental conditions

This section shows the main application of the model: determination of biofouling curves for brick surfaces exposed to time-variable environmental conditions. The brick is chosen in order to describe the most recurrent surface properties according to the literature review (Section 5.2.2): hence, P=0.19 and R=2.75 µm. For the sake of a better and more understanding of the application, only 5 different environmental conditions are determined, as reported in Table 7.2. These conditions are not real but the oscillation between the

temperature values allows to have distinctive types of curves that significantly differ from each other, as well as, the exposure to a constant environmental condition for 50 days helps to recognize the growth process for each temperature.

Environmental Condition	T [°C]	RH [%]	Time of exposure [day]
EC_1	14	100	50
EC_2	7.5	100	50
EC_3	20	100	50
EC_4	20	95	50
EC_5	27.5	100	50

Table 7.2. Summary of the environmental conditions and exposure time.

Figure 7.6 shows the process of the calculation T and RH depending curves, the determination of the time shifts for each environmental condition, the combination of each branch and hence, the overall resulting curve. In Figure 7.6 (a) the curves are determined for each T and RH values. Since the RH is lower than 98% the resulting curve is set to 0, while all the T values are between 5° and 40°C, hence, algae are able to grow, and their coverage can be determined. Figure 7.6 (b) shows the resulting values of time shift $t_{s,i}$ for each change in temperature. It is worth noting that the time shift is not determined for the EC_2 and EC_4: in fact, for both the EC, the previously reached covered area is higher than the A_C/A_T for T=7.5°C and RH=95%. Hence, the previously reached covered area is maintained constant for the whole duration of EC_2 and EC_4, since the algae cannot growth further, having already reached the relative maximum covered area. In addition, Figure 7.6 (c) graphically shows the calculation of the time shift and its effect: it allows to combine the curves by maintaining the same covered area at the moment of the change in environmental condition. Lastly, Figure 7.6 (d) shows the overall growth curve resulting from time varying T and RH. Shortly, Figure 7.6 (a) determines the curves depending on T and RH, Figure 7.6 (b) set the time shift for each change in environmental condition, that allow algae to grow further and Figure 7.6 (c) shows hot to combine the curves. Figure 7.6 (d) is the results of such process.

46
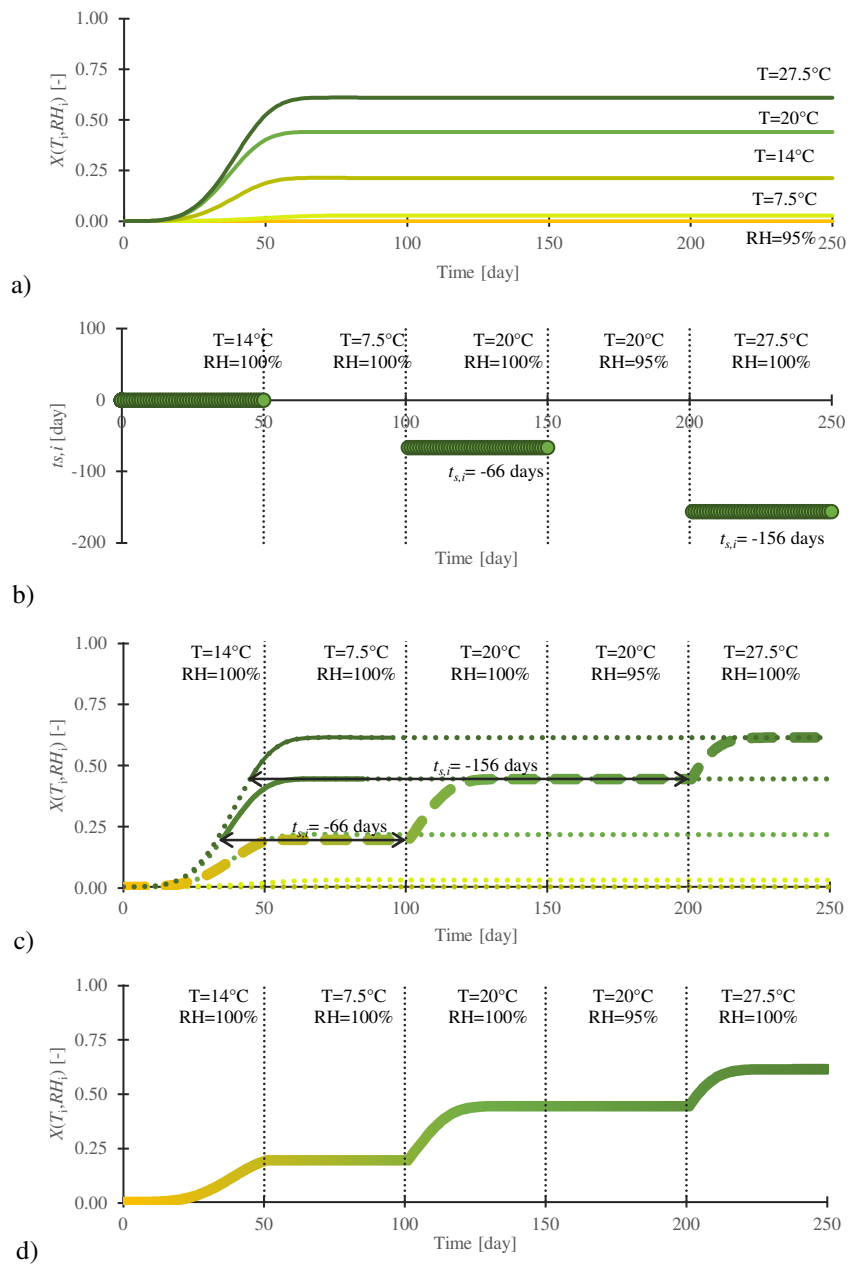
Figure 7.6. Determination process of algae growth under time varying *T* and *RH*: (a) algae growth curves according to *T* and *RH*; (b) time shift $t_{s,i}$ values; (c) time shift and curves combination; (d) the overall growth curve. The colour scale (yellow-green) indicates the increasing covered area by algae biofouling.

47

A real case application is shown in Figure 7.7, where T and RH are obtained as time history output of DELPHIN simulation software. The brick properties are unaltered, that is P=0.19 and R=2.75 µm. Figure 7.7 (a) shows the T and RH values for a year simulation; Figure 7.7 (b) reports the surface of algae growth according to T and t and Figure 7.7 (c) describes the time shift values for each change in T and RH. Hence, Figure 7.7 (d) shows the overall growth process for algae on brick as a resulting from the combination of the growth curve for each $T(t)$ and $RH(t)$ and their respective $t_{s,i}$ values.

a)

b)

c)

d)
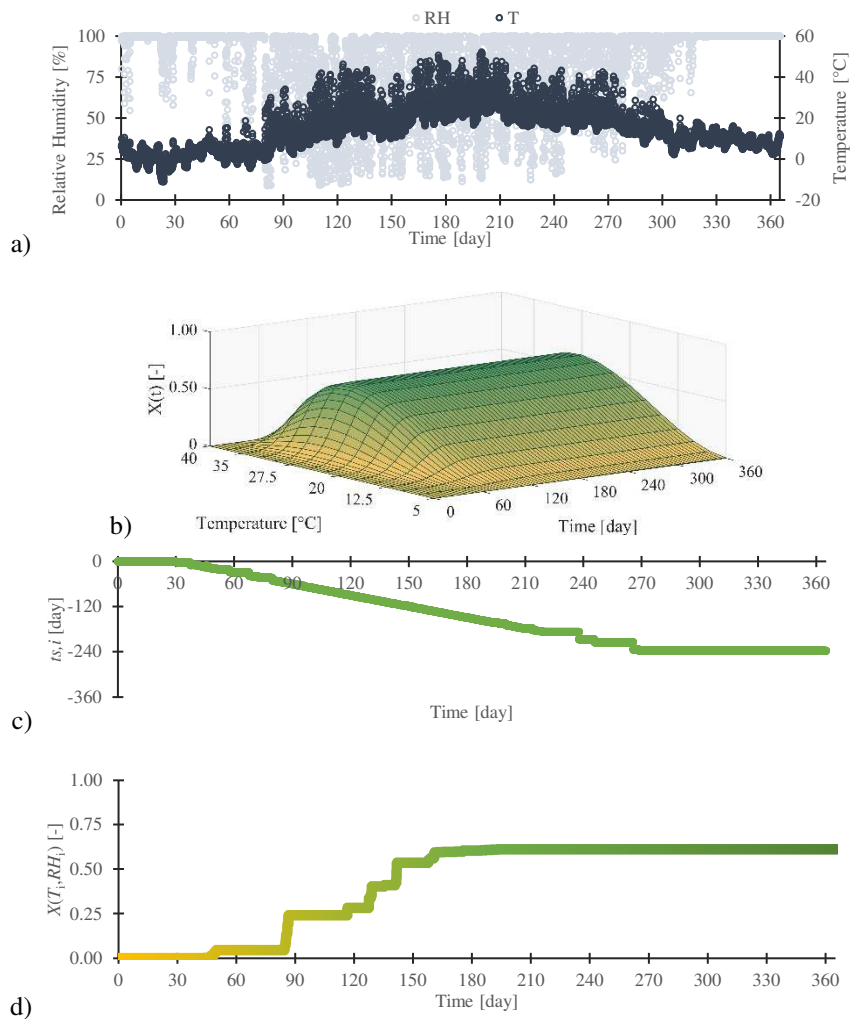
Figure 7.7. Determination process of algae growth for a real case scenario: (a) T and RH time history values; (b) algae growth surface according to T and RH; (c) time shift $t_{s,i}$ values; (d) the overall growth curve. The colour scale (yellow-green) indicates the increasing covered area by algae biofouling.

48

7.3.2 Application to different bricks surfaces from literature

A second application shows the capability of ALGAE model to predict biofouling on different bricks surfaces. Five bricks are chosen from literature with different combinations of porosity and roughness values [13,15,21,27,110,127]. The substrate properties of chosen bricks are reported in Table 7.3.

Name	Porosity [-]	Roughness [μm]
LRU	0.19	2.80
Untreated	0.21	7.22
FVE-1	0.31	6.00
FVE-2	0.34	5.47
FVE-3	0.36	7.99
Brick	0.39	3.80

Table 7.3. Substrate properties of fired brick surfaces from literature [13,15,21,27,110,127].

As shown in Figure 7.8, the proposed empirical failure model is able to determine the growth curves for each material for the entire temperature domain, taken as constant over the time. According to the model previsions, the material LRU (Figure 7.8 (a)) shows the best resistance to algae biofouling with a maximum covered area of about 0.50 for T=27.5°C. Conversely, materials FVE-1 and FVE-2 are the most favorable to algae growth: they reach almost the total biofouling in about 50 day, under the optimal temperature (Figure 7.8 (c-d)).
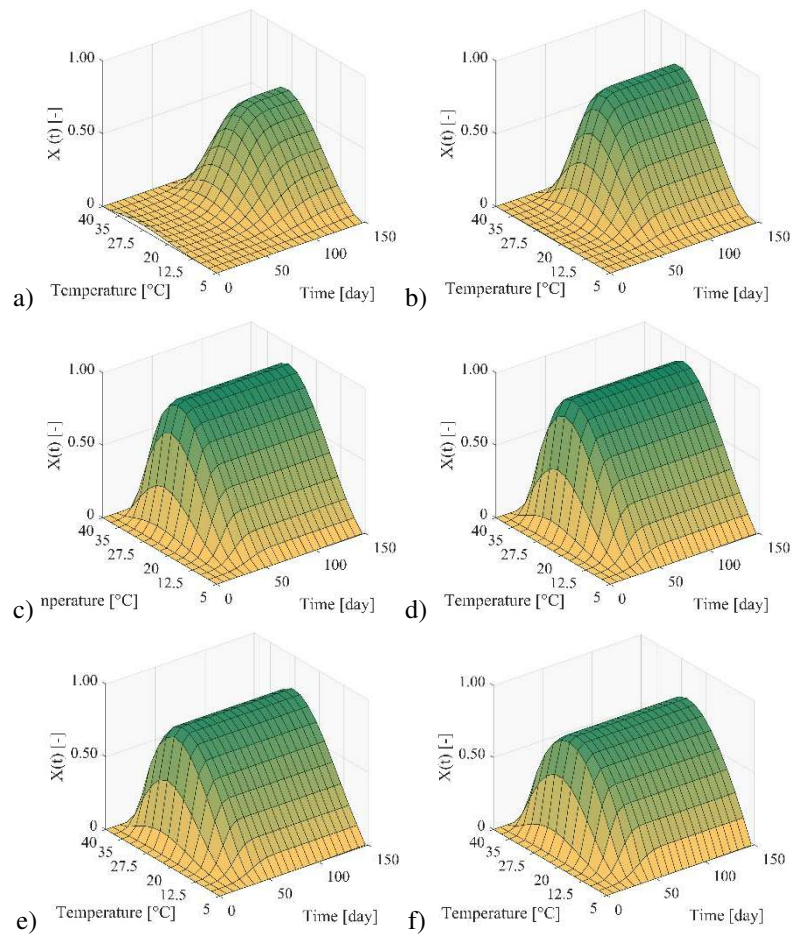
Figure 7.8. Application of the failure model to different types of fired bricks from literature [13,15,21,27,110,127] under the temperature domain. The colour scale (yellow-green) indicates the increasing covered area by algae biofouling.

50

Chapter 8

The logistic function: results of the comparisons

8.1 Overlapping the experimental data

Figure 8.1 shows the percentage of the values of the Avrami's and logistic model that falls within the minimum and maximum values of the experimental data. For fired brick (Figure 8.1 (a)), about the 2/3 of the Avrami's values fall within the given experimental range. For the logistic model, these values raise up to about 3/4. For the stony materials (Figure 8.1 (b)), results are reported together since limestones and sandstone have comparable result: both the models are comparable.

a)

b)
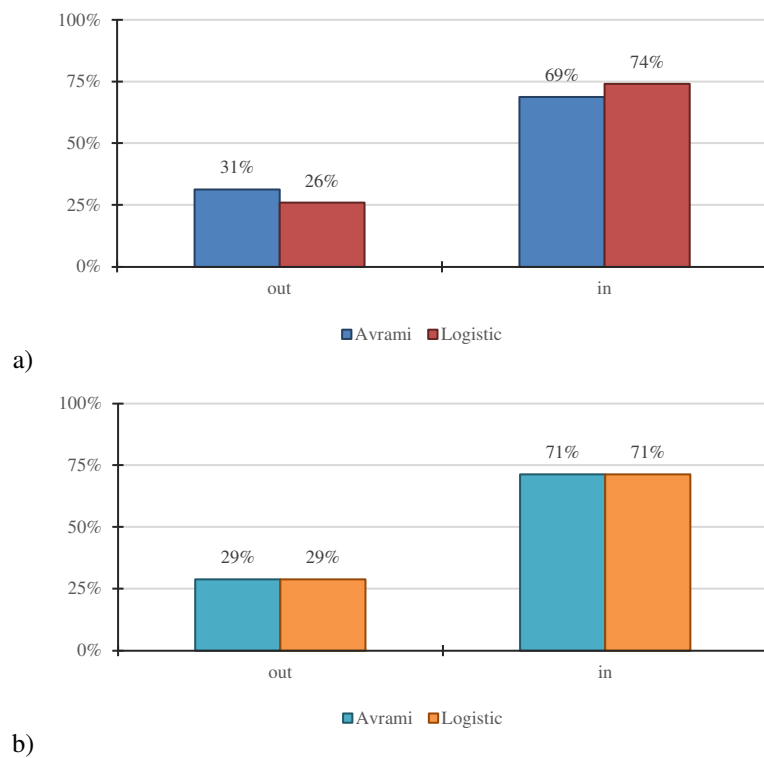
Figure 8.1. Analysis of Avrami's and logistic values within the experimental values for:
a) bricks; b) stones.

Figure 8.2 shows the scatter plots that compares the $R_\%$ obtained for both the models applied to fired bricks and stones. For fired bricks (Figure 8.2 (a)), it is evident that the logistic model presents better results: the $R_\%$ values are all below the bisector line of the graph. In particular, when the Avrami's model is less correct (2 treated bricks and 1 untreated) with $R_\%$ values ranging between 45% and 60%, the logistic model is able to increase the accuracy down to 10%). For stones, both models are, instead, highly precise since all the $R_\%$ are below 1%.

a)

b)
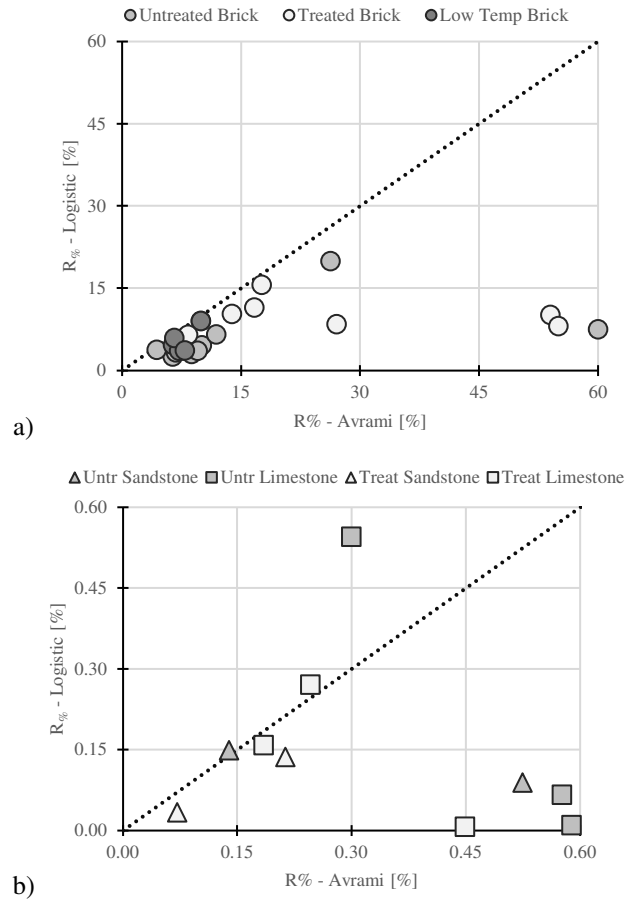
Figure 8.2. Comparative scatter plot between the Avrami's and the logistic function $R_\%$ parameter: a) fired bricks; b) sandstone (triangle) and limestone (square). Dotted line represents the graph bisector line.

When analyzing the trend of the values out for each phases (Figure 8.3 (b)) the first evidence is that both the model miss 1 experimental value out of 2 in the latency phase but the percentage values are comparable (44%-48%). The accuracy of the two models in lying inside the experimental values increased in the other two phases: the logistic almost halves the errors compared to the Avrami's values out both in the exponential and stagnation phase. Lastly, Figure 8.3 (c) shows that the main difference between the two model lies in the quantification of such values out: the logistic model reduces the overestimation and underestimation of the experimental data, especially in both the exponential and stagnation phases. The underestimation of the experimental values decreases from -60% up to -10% with the logistic model.

a)

b)
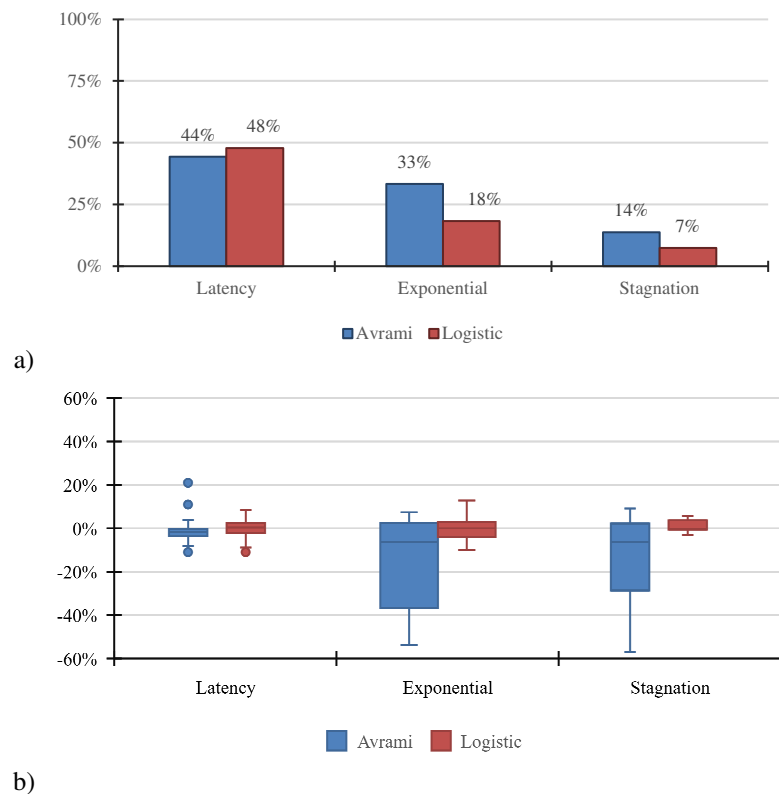
Figure 8.3. Analysis of Avrami's and logistic values out of the experimental range for bricks: a) trend correlation between values out and growth phases; b) boxplot analysis for under/overestimation trends.

For the stony materials, the models are comparable in all the two analyses, as shown in Figure 8.4. A slight difference can be noted only in the boxplot analysis where the logistic reduced the overestimation of the experimental data in the latency phase.

a)

b)
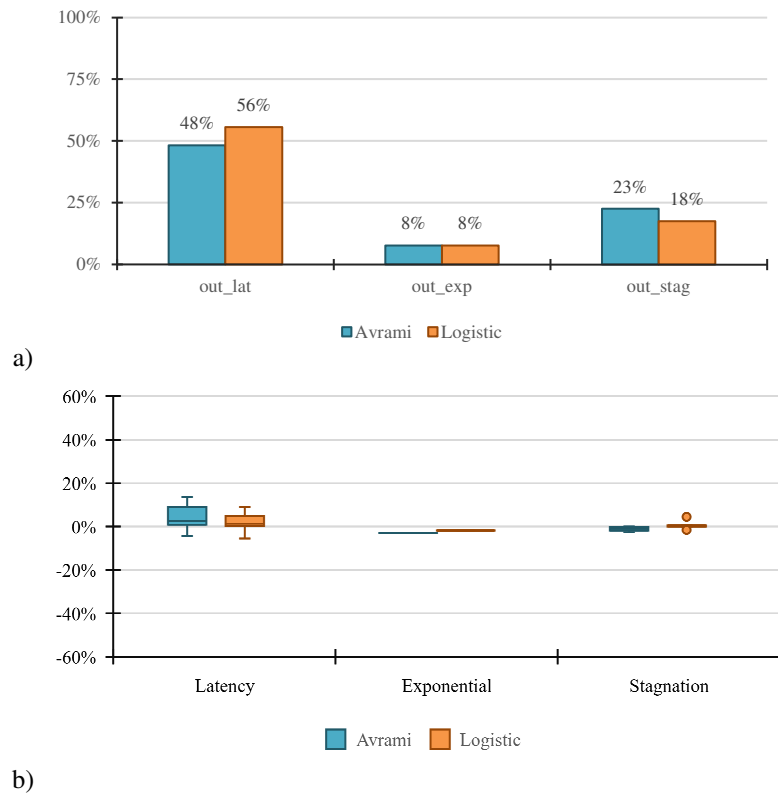
Figure 8.4. Analysis of Avrami's and logistic values within the experimental values for stones: a) total percentage; b) trend correlation between values out and growth phases; c) boxplot analysis for under/overestimation trends.

8.2 Overcoming the Avrami's flaws

The experimental data without the latency phase resulting in the collection are the ones solely referring to ANt, ACu and AAg materials, confirming what previously reported in literature [15]. For such materials, the logistic model better simulates the fast growth than the Avrami's model, as shown in Figure 8.5. Moreover, the starting point of the logistic model higher than 0 could take into account the combined effect of the inoculation method adopted in the experimental apparatus [15,25,27] and the very rough surface of the materials (Table 6.1).
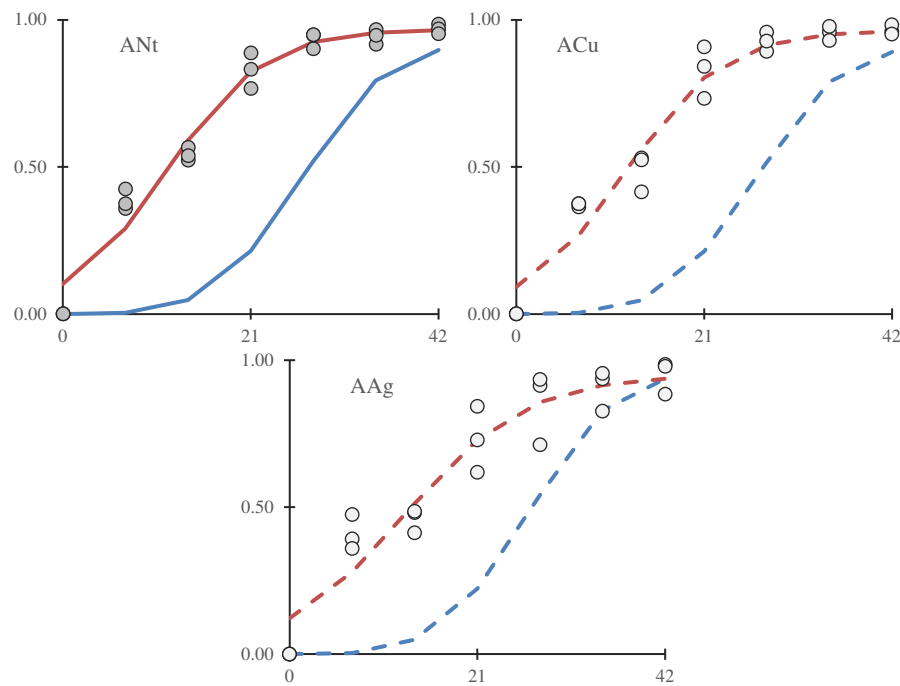
Figure 8.5. Overcoming the Avrami's flow: fast growth. Points indicate the experimental data under optimal growth conditions (grey) and treated (white); blue line indicates the Avrami's model; red line indicates the Logistic Function curve; dashed lines relatively indicate materials with surface treatments. X-axis represent the time of growth [day]; Y-axis represents the microalgae covered area $X(t)$ [-].

As previously demonstrated in such work, the logistic model is able to overcome the second Avrami's flaw thank to the difference in the analytical formulation that allows the first derivative to be always higher than 0 for every time value. Hence, the curve is always increasing- Nevertheless, Figure 8.6 shows one of the most significative scenario representing such problem and the simulating differences between the two models. Since the latency time t_l was set to 28 days, the Avrami's model had a slight decreasing trend with a starting point at about +0.05, while the logistic didn't.
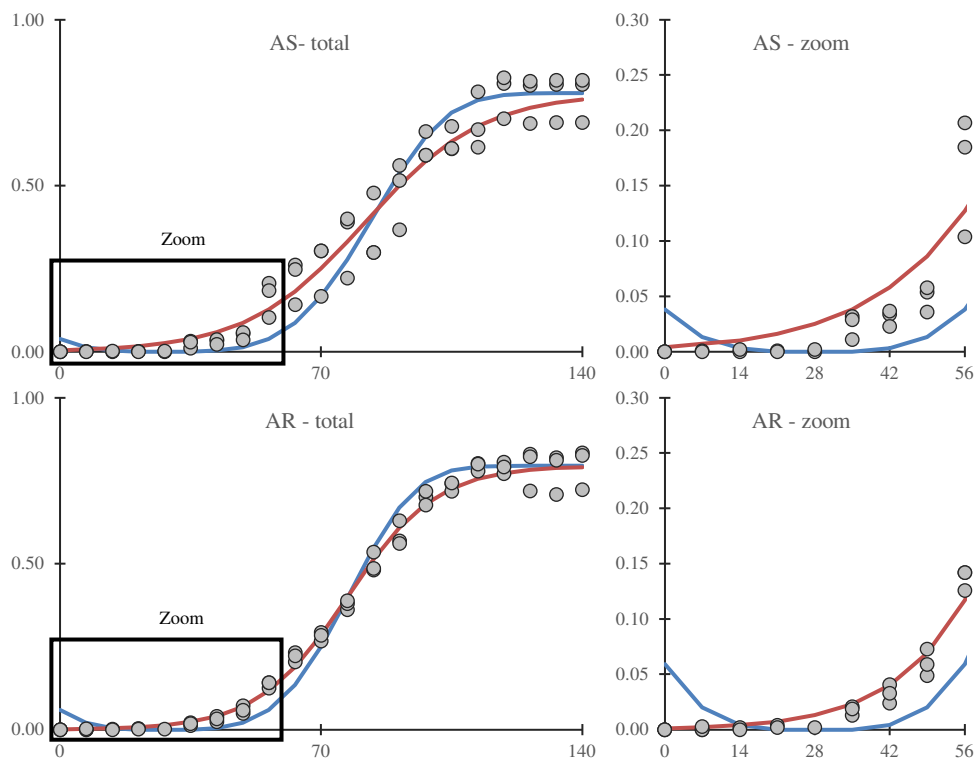
Figure 8.6. Comparison between average experimental data, Avrami's model curve and Logistic for materials AS-AR with slow growth [25]. Points indicate the average experimental data under optimal growth conditions (grey); blue line indicates the Avrami's model; red line indicates the Logistic Function curve. X-axis represent the time of growth [day]; Y-axis represents the microalgae covered area X(t) [-].

For sake of clarity, since the curves of the other bricks and stony materials (listed in Table 6.1and in Table 6.2) showed barely visible differences are not here reported, but they can be found in Appendix A.

8.3   Correlation with growth influencing factor

The first result of the correlation analysis is that the accuracy of both models for bricks is poorly affected by microalgae growth influencing factors (Figure 8.7) since all the obtained R^2 values are lower than 0.50. When comparing the two models, however, we can note that 8 logistic R^2 values out of 10 are lower than their Avrami's, for substrate properties and temperature. For surface treatments, the correlation is barely null for both of them. The only $R^2 \geq 0.50$ is the one between the values out during the exponential phase and the temperature for the Avrami's model.
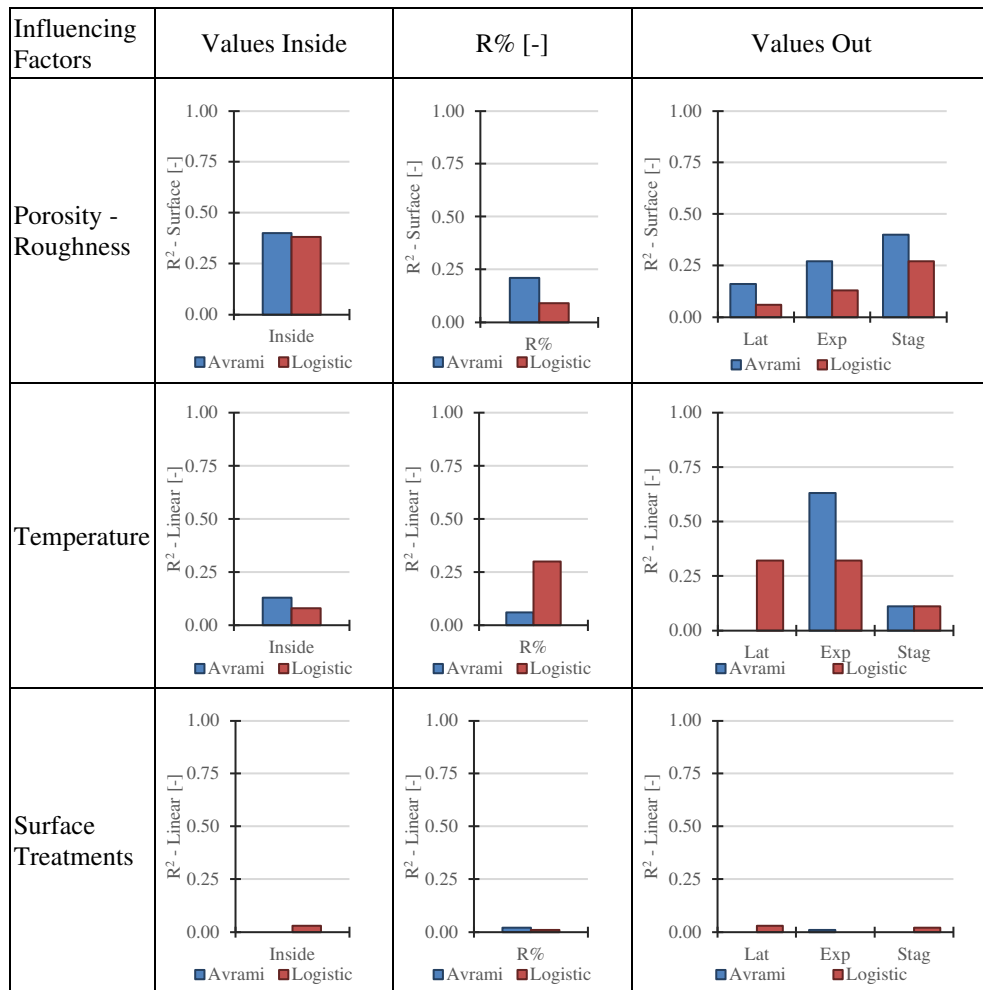
Figure 8.7. Correlation analysis (R^2) between the two model and the microalgae influencing factors for fired bricks. "Lat", "Exp" and "Stag" indicate respectively the latency, exponential and stagnation phase.

For what concerns the stony materials, results are reported together since limestones and sandstone have comparable result (Figure 8.8). In this case, however, a strong correlation between the substrate properties and the model accuracy can be observed. In particular, R^2 is way higher than 0.50 for the values inside and outside. Nevertheless, the logistic R^2 values are lower than the Avrami's one showing a weaker correlation. As for bricks, surface treatments have no influence on the models' accuracy.

Influencing Factors	Values Inside	R% [-]	Values Out
Porosity - Roughness			
Surface Treatments			
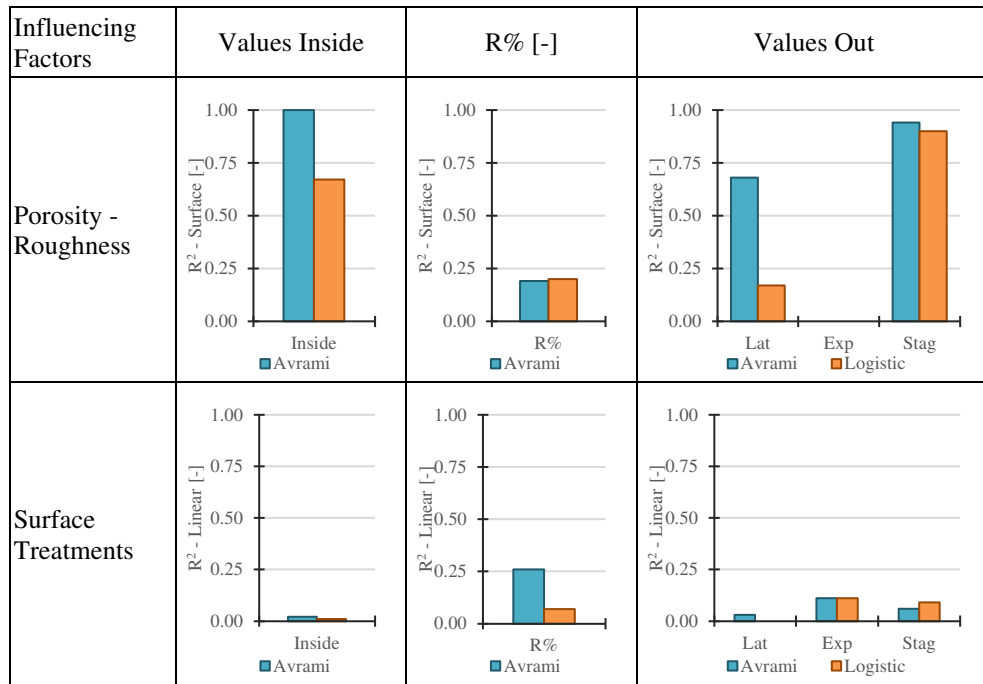
Figure 8.8. Correlation analysis (R^2) between the two model and the microalgae influencing factors for fired bricks. "Lat", "Exp" and "Stag" indicate respectively the latency, exponential and stagnation phase.

Figure 8.9 shows all the scatter plots for $R^2 \geq 0.50$. According to that, it is possible to note that for bricks, Avrami's model accuracy (in term of less values out) is higher for low temperature values. For stones, the substrate properties, mainly porosity, influence the numbers of outvalues especially the ones in the stagation phase. The lower the porosity is, the more correct the models are.

Laslty. it is possible to observe that, when $R^2 \leq 0.50$, e.g the $R^2 = 0.17$ for logistic values out in the latency phase with (Figure 8.9 (b)), datapoint are quite scattered, thus their determined trend are not predictive. Nevertheless, all the remaining trend, with $R^2 < 0.50$ for bricks and stones, are reported in Appendix B.

58
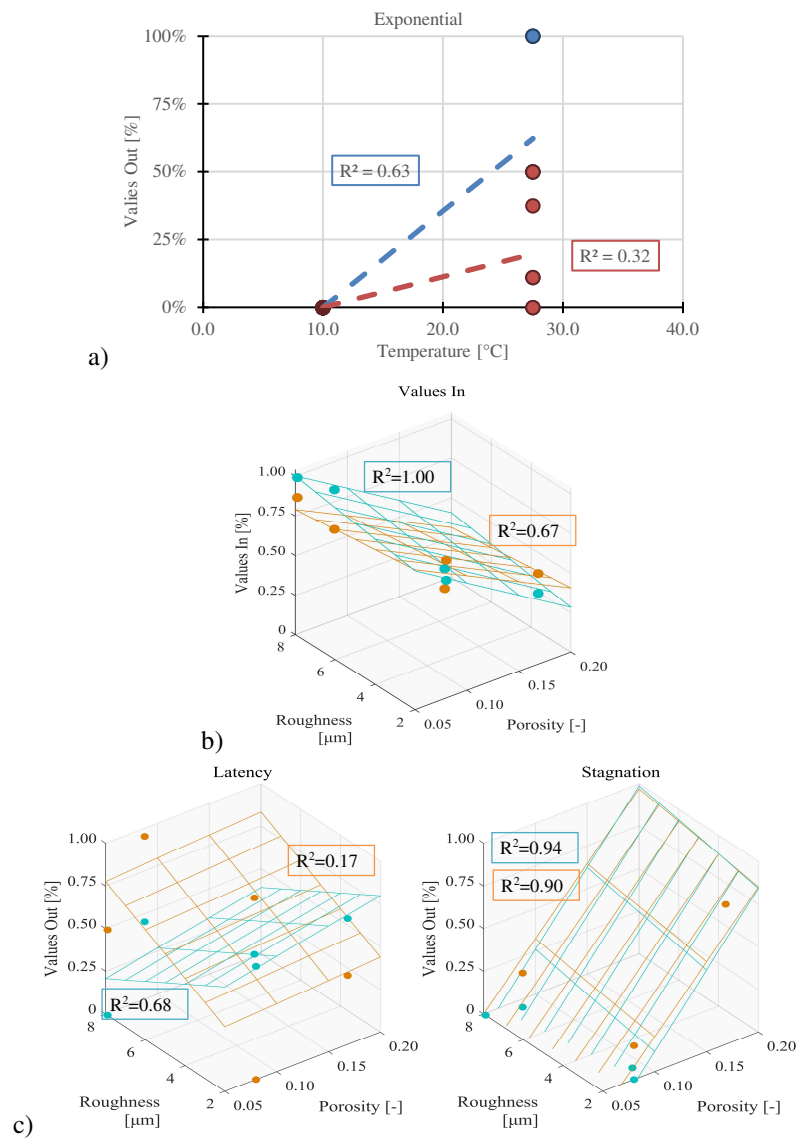
Figure 8.9. Trend analysis: scatter plot for $R^2 \geq 0.50$. (a) brick values out in exponential phase; (b) stone values in; (c) latency values out and stagnation values out.
Points indicate the determined values; mesh indicates the fitting results. Blu and light blue indicate the Avrami's model, red and light red indicate the logistic model, respectively for bricks and stones.

60

Chapter 9

Conclusions

Fired bricks are one of the materials that most frequently make up our buildings, both historic and modern. However, due to their rough surface and the internal high porous structure, they are often subject to biodeterioration phenomena, in particular by algae and cyanobacteria. These two microorganisms form on the outer layer of the material stains and patinas, mainly green and black, which aesthetically, physically and chemically alter the surface. In addition to this, the film formed by the microalgae allows the engraftment of bacteria, molds and fungi that can be severely harmful to human health. The degrading action of these organisms therefore entails serious cultural losses, when concerning building heritage, economic losses, due to frequent maintenance operations, and risks to the health of the occupants. Hence, failure models for biofouling on building materials have becoming a more and more unavoidable need: by making quantitative predictions, they can assist professionals and researchers in developing guidelines for interventions leading to a decrease in maintenance costs. Literature already provides such models for mold and fungi growth, but it is still limited to an empirical model for algae growth.

This work therefore tries to fill this gap by proposing a determined and validated a failure model for bricks. The model described here is able to simulate algae growth starting from the characteristics of the substrate when subjected to different conditions of temperature and relative humidity. As already proposed in the empirical model, these variables enter directly into the parameters of Avrami's theory, frequently applied in literature to describe the algae growth curve. From the obtained results, the model seems to be generally applicable since the tested domain of porosity and roughness covers more than 80% of the fired bricks reported in literature. In addition, the analytical definition of the dynamic model, proposed only graphically in the previous experimental model, allows the implementation of the model on simulation software. This will allow engineers and practitioners to make predictions according to real environmental conditions.

At the same time, in this work the logistic formula is compared to the Avrami's theory. The aim is the determination of a theory that may be truly capable of describing algae growth under all growth conditions, overcoming the Avrami's flaws. The comparison is made by using the same experimental dataset available in literature. The results show that the logistic model seems to be more reliable than the Avrami's model. In fact, it is: (1) accurate as the Avrami's model, or even more accurate when applied to bricks, in overlapping the experimental data, by reducing the over/underestimations and increasing the fitting quality; able (2) to overcome the Avrami's flaws both when the growth is too fast or too slow; (3) lesser or even not at all disturbed by the influencing factors for microalgae growth.

Future work should work jointly with these two approaches. The failure model based on the Avrami's theory should be tested on different bricks and/or environmental conditions, as soon as the experimental data will be available. Laboratory tests with varying temperature and relative humidity are also suggested in order to compared experimental data and the results from the failure model. This will fill the urgent need of a failure model for algae

growth. In parallel, a new version of the failure model could be developed considering the logistic formula as basic theory. Moreover, a first model extension to stony surfaces is recommended when experimental data will be available as well as to other building materials (e.g. plasters, mortars, ETICS) when such data will be presented.

Appendix A

Figure A. 1 reports all the logistic curves determined and applied to the literature experimental data and compared to the Avrami's curve for fired bricks materials [15,25,27]. Materials are listed according to Table 6.1.

a)

b)

c)

d)

e)
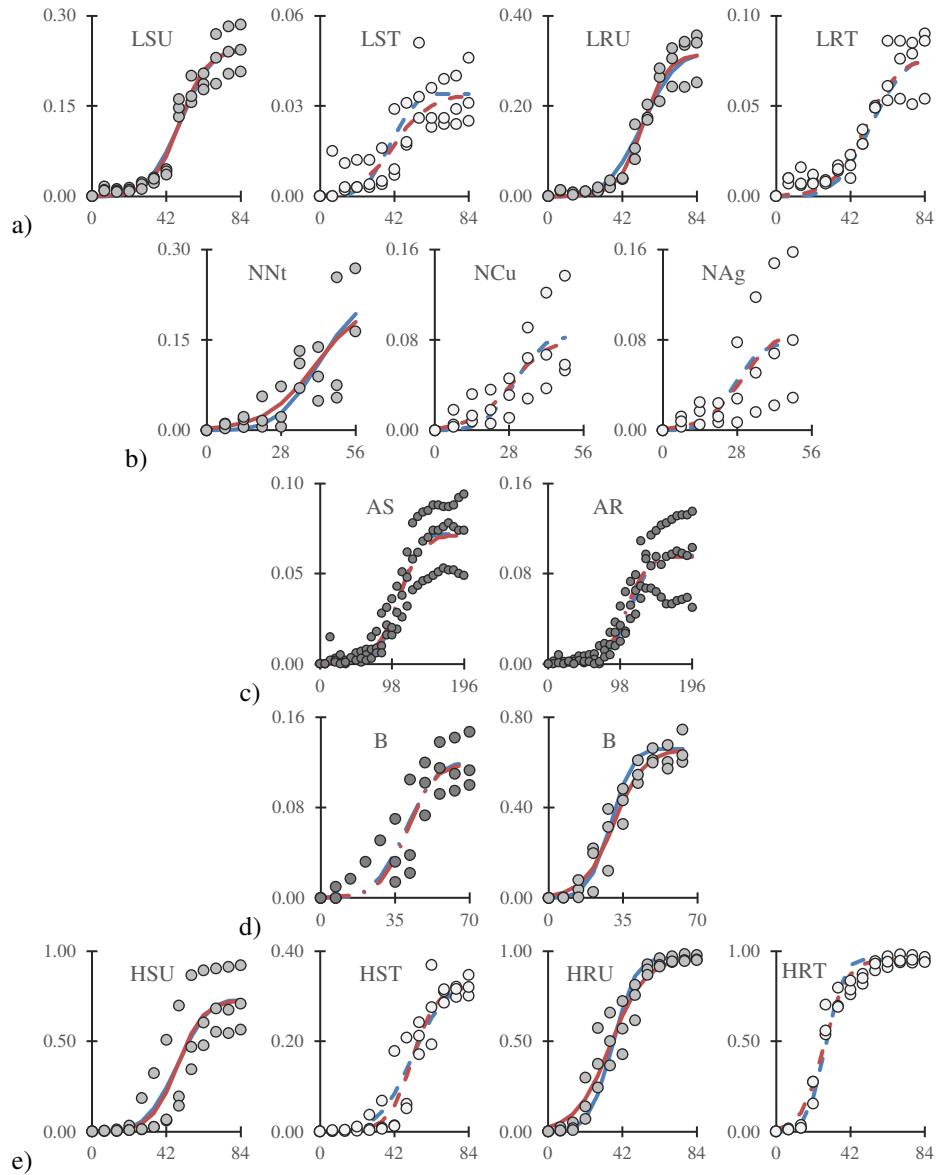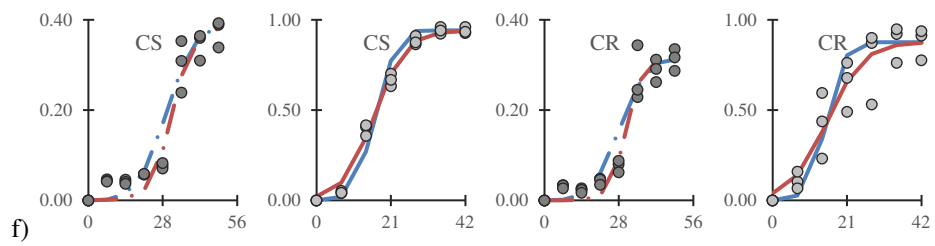
f)

Figure A. 1. Comparison between average experimental data, Avrami's model curve and Logistic Function curve for fired bricks [15,25,27], listed according to Table 6.1. Points indicate the average experimental data under optimal growth conditions (grey), under low temperature (dark grey) and treated (white); blue line indicates the Avrami's model; red line indicates the Logistic Function curve; dotted and dashed lines relatively indicate materials under low temperature and with surface treatments. X-axis represent the time of growth [day]; Y-axis represents the microalgae covered area X(t) [-].

Figure A. 2 shows the logistic curve determined and applied to the stony experimental data compared to the respective Avrami's curve [28]. Materials are listed according to Table 6.2.
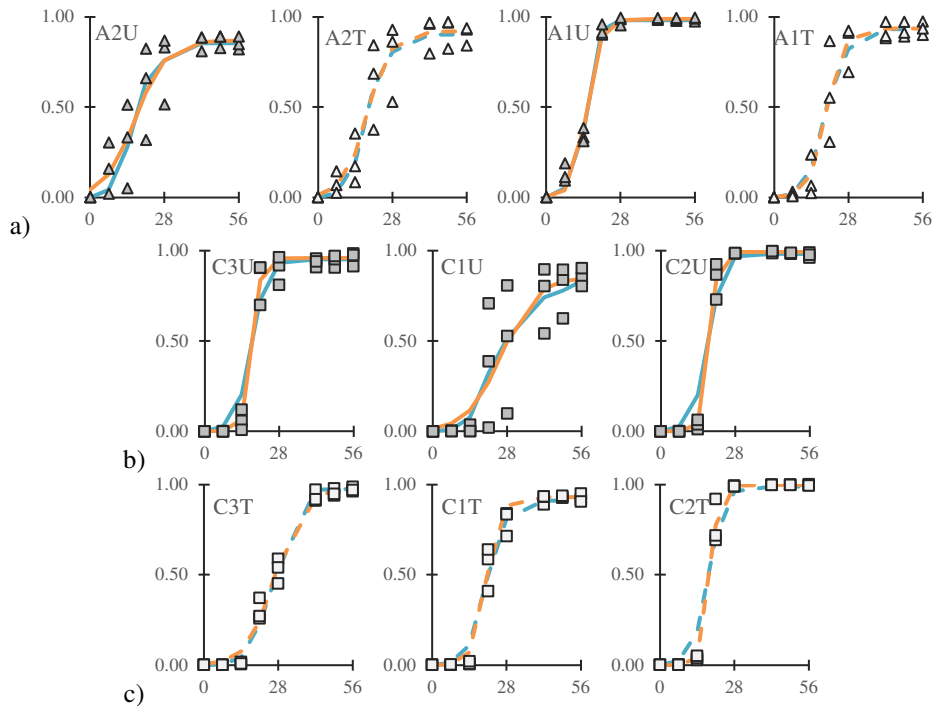
Figure A. 2. Comparison between average experimental data, Avrami's model curve and Logistic Function curve for stones [28]: (a) sandstone (triangle); (b-c) limestone (square). Points indicate the average experimental data under optimal growth conditions (grey) and treated (white); light blue line indicates the Avrami's model light red line indicates the Logistic Function curve; dashed lines relatively indicate materials with surface treatments. X-axis represent the time of growth [day]; Y-axis represents the microalgae covered area X(t)[-].

Appendix B

Figure B. 1 shows all the scatter plot and the determined trend for all the $R^2 \leq 0.50$ for the brick surfaces, indicating also their respective R^2.

a)

b)

c)

R²=0.21

R²=0.09

R² = 0.06

R² = 0.30

R² = 0.02

R² = 0.01

d)
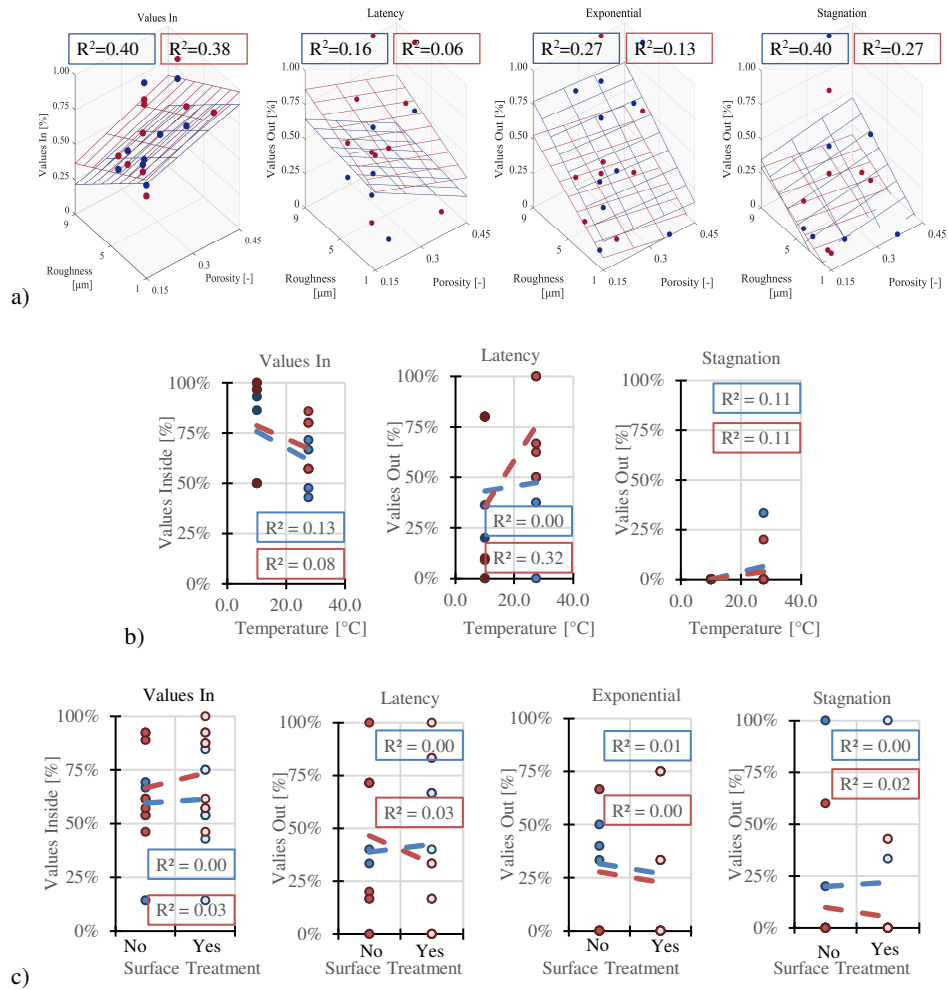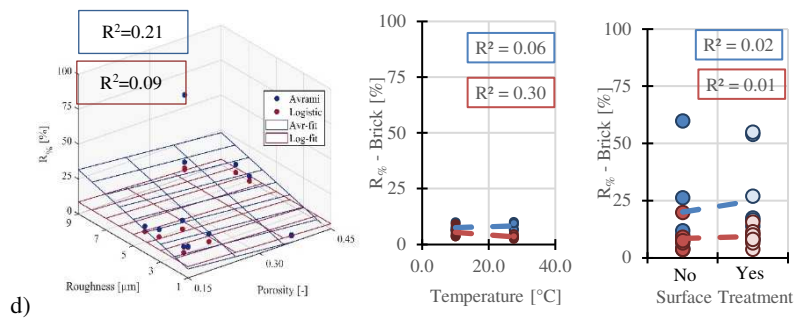
Figure B. 1. Correlation analysis for bricks: (a) Values in and out with Porosity and Roughness, (b) Values in and out with Temperature; (c) Values in and out with Surface treatment; (d) $R_\%$ with all the three influencing factors.
Points indicate the determined values, lines indicate the fitting results, respectively blue for Avrami's model and red for the logistic.

Figure B. 2 shows all the scatter plot and the determined trend for all the $R^2 \leq 0.50$ for the stony materials, indicating also their respective R^2.

a)

b)

c)
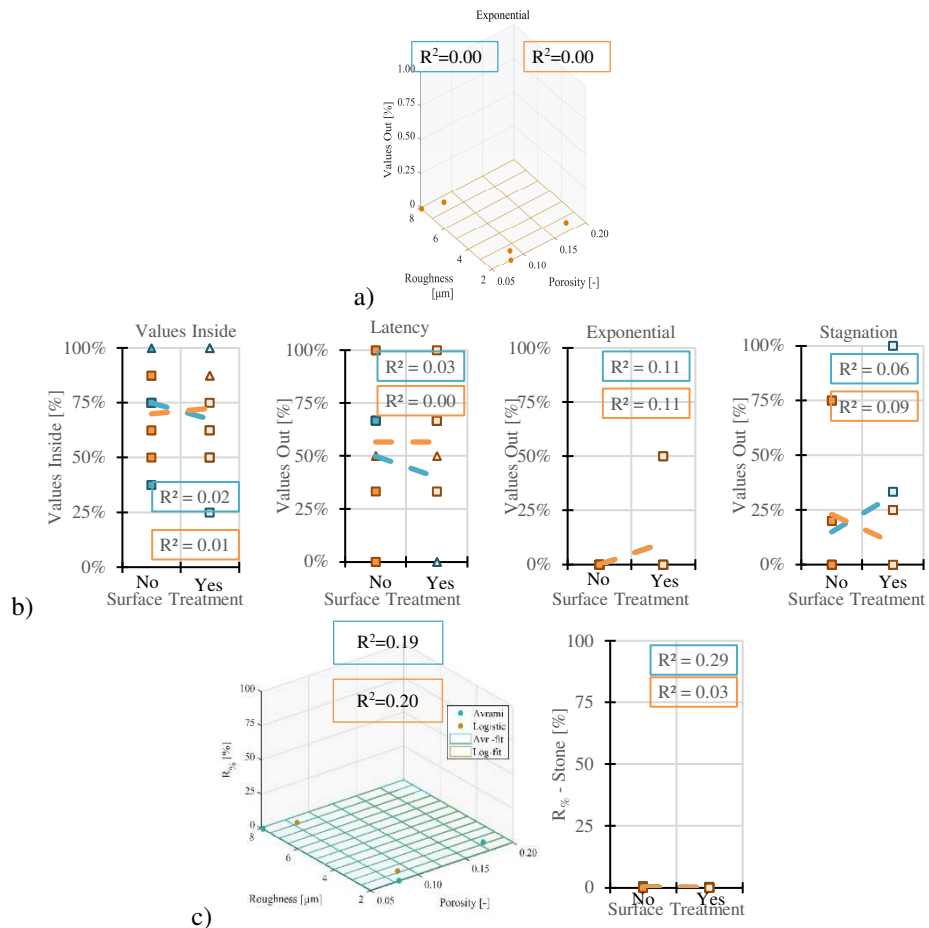
Figure B. 2. Correlation analysis for stones: (a) Values in and out with Porosity and Roughness, (b) Values in and out with Surface treatment; (c) $R_\%$ with all the three influencing factors. Points indicate the determined values, lines indicate the fitting results, respectively light blue for Avrami's model and light red for the logistic.

70

References

[1]   G. Caneva, M.P. Nugari, O. Salvadori, Biology in the Conservation of Works of Art, ICCROM, 1991.

[2]   G. Torraca, Lectures on Materials Science for Architectural Conservation, Los Angeles, 2009.

[3]   E. Doehne, C.A. Price, Stone Conservation: An Overview of Current Research, 2010.

[4]   T. Warscheid, J. Braams, Biodeterioration of stone: a review, Int. Biodeterior. Biodegradation. 46 (2000) 343–368. doi:10.1016/S0964-8305(00)00109-8.

[5]   P. Tiano, Biodegradation of Cultural Heritage: Decay Mechanisms and Control Methods, 9th ARIADNE Work. "Historic Mater. Their Diagnostic." (2002) 1–37. doi:10.1.1.129.3386.

[6]   C. Gervais, C. Grissom, C. McNamara, N.R. Konkol, R. Mitchell, Biocolonization of Stone: Control and Preventive Methods, Biocolonization Stone Control Prev. Methods Proc. from MCI Work. Ser. (2011) 87–90. doi:10.5479/si.19492359.2.1.

[7]   H. Viitanen, J. Vinha, K. Salminen, T. Ojanen, R. Peuhkuri, L. Paajanen, K. Lähdesmäki, Moisture and bio-deterioration risk of building materials and structures, J. Build. Phys. 33 (2010) 201–224. doi:10.1177/1744259109343511.

[8]   E. Pieckovà, Z. Jesenskà, Microscopoc fungi in dwellings and their health implications in humans, Ann Agric Env. Med. 6 (1999) 1–11. doi:10.2989/salals.2009.27.3.1.935.

[9]   S.D. Platt, C.J. Martin, S.M. Hunt, C.W. Lewis, Damp housing, mould growth, and symptomatic health state, Br. Med. J. 298 (1989) 1673–1678. doi:10.1136/bmj.298.6689.1673.

[10]   M.L. Coutinho, A.Z. Miller, M.F. Macedo, Biological colonization and biodeterioration of architectural ceramic materials: An overview, J. Cult. Herit. 16 (2015) 759–777. doi:10.1016/j.culher.2015.01.006.

[11]   C. Coletti, G. Cultrone, L. Maritan, C. Mazzoli, How to face the new industrial challenge of compatible, sustainable brick production: Study of various types of commercially available bricks, Appl. Clay Sci. 124–125 (2016) 219–226. doi:10.1016/J.CLAY.2016.02.014.

[12]   A.Z. Miller, A. Dionísio, L. Laiz, M.F. Macedo, C. Saiz-Jimenez, The influence of inherent properties of building limestones on their bioreceptivity to phototrophic

microorganisms, Ann. Microbiol. 59 (2009) 705–713. https://link.springer.com/content/pdf/10.1007%2FBF03179212.pdf.

[13]   P. Tiano, P. Accolla, L. Tomaselli, Phototrophic biodeteriogens on lithoid surfaces: An ecological study, Microb. Ecol. 29 (1995) 299–309. doi:10.1007/BF00164892.

[14]   O. Guillitte, Bioreceptivity: a new concept for building ecology studies, Sci. Total Environ. 167 (1995) 215–220. doi:10.1016/0048-9697(95)04582-L.

[15]   L. Graziani, E. Quagliarini, M. D'Orazio, The role of roughness and porosity on the self-cleaning and anti-biofouling efficiency of TiO2-Cu and TiO2-Ag nanocoatings applied on fired bricks, Constr. Build. Mater. 129 (2016) 116–124. doi:10.1016/j.conbuildmat.2016.10.111.

[16]   L. Graziani, E. Quagliarini, A. Osimani, L. Aquilanti, F. Clementi, M. D'Orazio, The influence of clay brick substratum on the inhibitory efficiency of TiO2 nanocoating against biofouling, Build. Environ. 82 (2014) 128–134. doi:10.1016/j.buildenv.2014.08.013.

[17]   S. Johansson, Biological growth on mineral façades, 2005.

[18]   C. Ferrari, G. Santunione, A. Libbra, A. Muscio, E. Sgarbi, C. Siligardi, G.S. Barozzi, Review on the influence of biological deterioration on the surface properties of building materials: Organisms, materials, and methods, Int. J. Des. Nat. Ecodynamics. 10 (2015) 21–39. doi:10.2495/DNE-V10-N1-21-39.

[19]   E. Imre Friedmann, R. Ocampo-Friedmann, A primitive cyanobacterium a pioneer microorganism for terraforming mars, (1995).

[20]   K. Lengsfeld, M. Krus, Microorganism on façades – reasons, consequences and measures, (2001) 0–7.

[21]   M. D'Orazio, G. Cursio, L. Graziani, L. Aquilanti, A. Osimani, F. Clementi, C. Yéprémian, V. Lariccia, S. Amoroso, Effects of water absorption and surface roughness on the bioreceptivity of ETICS compared to clay bricks, Build. Environ. 77 (2014) 20–28. doi:10.1016/j.buildenv.2014.03.018.

[22]   L. Graziani, E. Quagliarini, M. D'Orazio, Application of titania nanocoating to clay brick façades for biofouling prevention: efficiency and effect of substratum, Colloqui.AT.E. 1 (2014) 6.

[23]   L. Graziani, M. D'Orazio, Biofouling prevention of ancient brick surfaces by TiO 2 -based nano-coatings, Coatings. 5 (2015) 357–365. doi:10.3390/coatings5030357.

[24]   L. Graziani, E. Quagliarini, M. D'Orazio, Superfici autopulenti e biocide nel

72

Restauro Archeologico di pietre e laterizi, Restauro Archeol. 2 (2016) 22–43. doi:10.13128/RA-19508.

[25]   E. Quagliarini, A. Gianangeli, M. D'Orazio, B. Gregorini, A. Osimani, L. Aquilanti, F. Clementi, Effect of temperature and relative humidity on algae biofouling on different fired brick surfaces, Constr. Build. Mater. 199 (2019) 396–405. doi:10.1016/J.CONBUILDMAT.2018.12.023.

[26]   T.H. Tran, A. Govin, R. Guyonnet, P. Grosseau, C. Lors, D. Damidot, O. Devès, B. Ruot, Avrami's law based kinetic modeling of colonization of mortar surface by alga Klebsormidium flaccidum, Int. Biodeterior. Biodegrad. 79 (2013) 73–80. doi:10.1016/j.ibiod.2012.12.012.

[27]   L. Graziani, E. Quagliarini, M. D'Orazio, TiO2-treated different fired brick surfaces for biofouling prevention: Experimental and modelling results, Ceram. Int. 42 (2016) 4002–4010. doi:10.1016/j.ceramint.2015.11.069.

[28]   L. Graziani, E. Quagliarini, On the Modelling of Algal Biofouling Growth on Nano-TiO2 Coated and Uncoated Limestones and Sandstones, Coatings. 8 (2018) 54. doi:10.3390/coatings8020054.

[29]   J. Berger, H. Le Meur, D. Dutykh, D.M. Nguyen, A.C. Grillet, Analysis and improvement of the VTT mold growth model: Application to bamboo fiberboard, Build. Environ. 138 (2018) 262–274. doi:10.1016/j.buildenv.2018.03.031.

[30]   S.Y. Lee, B. Lei, B. Mallick, Estimation of COVID-19 spread curves integrating global data and borrowing information, PLoS One. 15 (2020) 1–17. doi:10.1371/journal.pone.0236860.

[31]   W. Kong, S. Huang, F. Shi, J. Zhou, Y. Feng, Y. Xiao, Study on Microcystis aeruginosa growth in incubator experiments by combination of Logistic and Monod functions, Algal Res. 35 (2018) 602–612. doi:10.1016/J.ALGAL.2018.10.005.

[32]   A. Gianangeli, A novel failure model to predict biofouling (algae growth) on different building facades under different environmental conditions, (2019).

[33]   Q. Wang, T. Zhang, Review of mathematical models for biofilms, Solid State Commun. 150 (2010) 1009–1022. doi:10.1016/J.SSC.2010.01.021.

[34]   K. Gradeci, N. Labonnote, B. Time, J. Köhler, A probabilistic-based methodology for predicting mould growth in façade constructions, Build. Environ. 128 (2018) 33–45. doi:10.1016/J.BUILDENV.2017.11.021.

[35]   T. Verdier, M. Coutand, A. Bertron, C. Roques, A review of indoor microbial growth across building materials and sampling and analysis methods, Build. Environ. 80

(2014) 136–149. doi:10.1016/J.BUILDENV.2014.05.030.

[36]   G. Arya, J. Singh, A mathematical model to predict Actinomycetes growth in building material, Int. J. Interdiscip. Res. Innov. 4 (2016) 88–96.

[37]   S. Thelandersson, T. Isaksson, Mould resistance design (MRD) model for evaluation of risk for microbial growth under varying climate conditions, Build. Environ. 65 (2013) 18–25. doi:10.1016/J.BUILDENV.2013.03.016.

[38]   T. Ojanen, R. Peuhkuri, Viitanen, Lähdesmäki, Vinha, Salminen, Classification of material sensitivity–new approach for mould growth modeling, … Nord. Symp. …. 2   (2011)   867–874. http://webhotel2.tut.fi/nsb2011/sites/webhotel2.tut.fi.nsb2011/files/b10_02_tuomo_ ojanen_vtt_nordic_9th_classification__mould_growth_final2.pdf.

[39]   M. Harrestrup, S. Svendsen, Internal insulation applied in heritage multi-storey buildings with wooden beams embedded in solid masonry brick façades, Build. Environ. 99 (2016) 59–72. doi:10.1016/J.BUILDENV.2016.01.019.

[40]   S. Fantucci, F. Isaia, V. Serra, M. Dutto, Insulating coat to prevent mold growth in thermal   bridges,   Energy   Procedia.   134   (2017)   414–422. doi:10.1016/J.EGYPRO.2017.09.591.

[41]   M. D'Orazio, G. Maracchini, An experimental investigation on the indoor hygrothermal environment of a reinforced-EPS based temporary housing solution, Energy Build. 204 (2019) 109500. doi:10.1016/J.ENBUILD.2019.109500.

[42]   G.C.J. Lynch, The Hystory of Gauged Brickwork, 1st Editio, 2007.

[43]   D. Hamilton, The Thames and Hudson manual of architectural ceramics, Thames and Hudson, London, 1978.

[44]   E. Sassoni, S. Andreotti, A. Bellini, B. Mazzanti, M.C. Bignozzi, C. Mazzotti, E. Franzoni, Influence of mechanical properties, anisotropy, surface roughness and porosity of brick on FRP debonding force, Compos. Part B Eng. 108 (2017) 257–269. doi:10.1016/J.COMPOSITESB.2016.10.020.

[45]   G. Cultrone, F. Madkour, Evaluation of the effectiveness of treatment products in improving the quality of ceramics used in new and historical buildings, J. Cult. Herit. 14 (2013) 304–310. doi:10.1016/J.CULHER.2012.08.001.

[46]   O. Guillitte, R. Dreesen, Laboratory chamber studies and petrographical analysis as bioreceptivity assessment tools of building materials, Sci. Total Environ. 167 (1995) 365–374. doi:10.1016/0048-9697(95)04596-S.

[47]   C. Gaylarde, M. Ribas Silva, T. Warscheid, Microbial impact on building materials: an overview, Mater. Struct. 36 (2003) 342–352. doi:10.1007/BF02480875.

[48]   A.Z. Miller, P. Sanmartín, L. Pereira-Pardo, A. Dionísio, C. Saiz-Jimenez, M.F. Macedo, B. Prieto, Bioreceptivity of building stones: A review, Sci. Total Environ. 426 (2012) 1–12. doi:10.1016/j.scitotenv.2012.03.026.

[49]   E. Quagliarini, A. Gianangeli, M. D'Orazio, B. Gregorini, A. Osimani, L. Aquilanti, F. Clementi, Effect of temperature and relative humidity on algae biofouling on different fired brick surfaces, Constr. Build. Mater. 199 (2019) 396–405. doi:10.1016/J.CONBUILDMAT.2018.12.023.

[50]   C. Saiz-Jimenez, Biodeterioration vs biodegradation: The role of microorganisms in the removal of pollutants deposited on historic buildings, Int. Biodeterior. Biodegrad. 40 (1997) 225–232. doi:10.1016/S0964-8305(97)00035-8.

[51]   C. Saiz-Jimenez, Biodeterioration of stone in historic buildings and monuments, Mycotoxins, Wood Decay, Plant Stress. Biocorrosion, Gen. Biodeterior. (1994) 587–604.

[52]   R. Kumar, A. V Kumar, Biodeterioration of Stone in Tropical Environments, 1999. doi:10.2307/1504678.

[53]   H.J. Hueck, The biodeterioration of materials as a part of hylobiology, 1965. https://www.narcis.nl/publication/RecordID/oai:tudelft.nl:uuid:cd2e06b7-2a61-4685-96b9-08a490c6e2c0.

[54]   I. Flores-Colen, J. de Brito, V.P. de Freitas, Stains in facades' rendering - Diagnosis and maintenance techniques' classification, Constr. Build. Mater. 22 (2008) 211–221. doi:10.1016/j.conbuildmat.2006.08.023.

[55]   E. Quagliarini, L. Graziani, D. Diso, A. Licciulli, M. D'Orazio, Is nano-TiO2 alone an effective strategy for the maintenance of stones in Cultural Heritage?, J. Cult. Herit. 30 (2018) 81–91. doi:10.1016/j.culher.2017.09.016.

[56]   S. Sanchez-Moral, L. Luque, S. Cuezva, V. Soler, D. Benavente, L. Laiz, J.M. Gonzalez, C. Saiz-Jimenez, Deterioration of building materials in Roman catacombs: The influence of visitors, Sci. Total Environ. 349 (2005) 260–276. doi:10.1016/j.scitotenv.2004.12.080.

[57]   T. Dornieden, A.A. Gorbushina, W.E. Krumbein, PATINA - Physical and Chemical Interactions of Sub-aerial Biofilms with Objects of Art, in: O. Ciferri, P. Tiano, G. Mastromei (Eds.), Microbes Art, Springer, Boston, MA, 2000: pp. 105–106. doi:https://doi.org/10.1007/978-1-4615-4239-1_8.

[58]   J.A. Clarke, C.M. Johnstone, N.J. Kelly, R.C. McLean, J.A. Anderson, N.J. Rowan, J.E. Smith, A technique for the prediction of the conditions leading to mould growth in buildings, Build. Environ. 34 (1999) 515–521. doi:10.1016/S0360-1323(98)00023-7.

[59]   I. Groth, R. Vettermann, B. Schuetze, P. Schumann, C. Saiz-Jimenez, Actinomycetes in Karstic caves of northern Spain (Altamira and Tito Bustillo), J. Microbiol. Methods. 36 (1999) 115–122. doi:10.1016/S0167-7012(99)00016-0.

[60]   F. Bourges, P. Genthon, D. Genty, M. Lorblanchet, E. Mauduit, D. D'Hulst, Conservation of prehistoric caves and stability of their inner climate: Lessons from Chauvet and other French caves, Sci. Total Environ. 493 (2014) 79–91. doi:10.1016/j.scitotenv.2014.05.137.

[61]   C.C. Gaylarde, P.M. Gaylarde, A comparative study of the major microbial biomass of biofilms on exteriors of buildings in Europe and Latin America, Int. Biodeterior. Biodegrad. 55 (2005) 131–139. doi:10.1016/j.ibiod.2004.10.001.

[62]   J.J. Ortega-Calvo, X. Ariño, M. Hernandez-Marine, C. Saiz-Jimenez, Factors affecting the weathering and colonization of monuments by phototrophic microorganisms, Sci. Total Environ. 167 (1995) 329–341. doi:10.1016/0048-9697(95)04593-P.

[63]   F. Borderie, L. Alaoui-Sehmer, F. Bousta, B. Alaoui-Sossé, L. Aleya, Cellular and molecular damage caused by high UV-C irradiation of the cave-harvested green alga Chlorella minutissima: Implications for cave management, Int. Biodeterior. Biodegrad. 93 (2014) 118–130. doi:10.1016/j.ibiod.2014.05.014.

[64]   F. Borderie, A.S. Laurence, R. Naoufal, B. Faisl, O. Geneviève, R. Dominique, A.S. Badr, UV-C irradiation as a tool to eradicate algae in caves, Int. Biodeterior. Biodegrad. 65 (2011) 579–584. doi:10.1016/j.ibiod.2011.02.005.

[65]   F. Borderie, N. Tête, D. Cailhol, L. Alaoui-Sehmer, F. Bousta, D. Rieffel, L. Aleya, B. Alaoui-Sossé, Factors driving epilithic algal colonization in show caves and new insights into combating biofilm development with UV-C treatments, Sci. Total Environ. 484 (2014) 43–52. doi:10.1016/j.scitotenv.2014.03.043.

[66]   H. Barberousse, B. Ruot, C. Yéprémian, G. Boulon, An assessment of façade coatings against colonisation by aerial algae and cyanobacteria, Build. Environ. 42 (2007) 2555–2561. doi:10.1016/j.buildenv.2006.07.031.

[67]   E. Vereecken, S. Roels, Review of mould prediction models and their influence on mould risk evaluation, Build. Environ. 51 (2012) 296–310. doi:10.1016/j.buildenv.2011.11.003.

76

[68]   E. Vereecken, D. Saelens, S. Roels, A comparison of different mould prediction models, Proc. Build. Simul. 2011 12th Conf. Int. Build. Perform. Simul. Assoc. 6 (2011) 1934–1941. http://www.scopus.com/inward/record.url?eid=2-s2.0-84870177840&partnerID=tZOtx3y1.

[69]   H. Barberousse, R.J. Lombardo, G. Tell, A. Couté, Factors involved in the colonisation of building façades by algae and cyanobacteria in France, Biofouling. 22 (2006) 69–77. doi:10.1080/08927010600564712.

[70]   L. Graziani, E. Quagliarini, M. D'Orazio, Application of titanium dioxide on clay brick façades for algal growth prevention, Int. Mason. Conf. 2014. (2014) 1–9.

[71]   D. Giovannacci, C. Leclaire, M. Horgnies, M. Ellmer, J.D. Mertz, G. Orial, J. Chen, F. Bousta, Algal colonization kinetics on roofing and façade tiles: Influence of physical parameters, Constr. Build. Mater. 48 (2013) 670–676. doi:10.1016/j.conbuildmat.2013.07.034.

[72]   T.H. Tran, A. Govin, R. Guyonnet, P. Grosseau, C. Lors, D. Damidot, O. Deves, B. Ruot, Influence of the intrinsic characteristics of mortars on their biofouling by pigmented organisms: Comparison between laboratory and field-scale experiments, Int. Biodeterior. Biodegrad. 86 (2014) 334–342. doi:10.1016/j.ibiod.2013.10.005.

[73]   A.Z. Miller, N. Leal, L. Laiz, M.A. Rogerio-Candelera, R.J.C. Silva, A. Dionísio, M.F. Macedo, C. Saiz-Jimenez, Primary bioreceptivity of limestones used in southern European monuments, Geol. Soc. Spec. Publ. 331 (2010) 79–92. doi:10.1144/SP331.6.

[74]   S.P. Singh, P. Singh, Effect of temperature and light on the growth of algae species: A review, Renew. Sustain. Energy Rev. 50 (2015) 431–444. doi:10.1016/j.rser.2015.05.024.

[75]   A. Konopka, T.D. Brock, Effect of temperature on blue-green algae (Cyanobacteria) in Lake Mendota, Appl. Environ. Microbiol. 36 (1978) 572–576. doi:10.1520/C1421-10.2.

[76]   R. Serra-Maia, O. Bernard, A. Gonçalves, S. Bensalem, F. Lopes, Influence of temperature on Chlorella vulgaris growth and mortality rates in a photobioreactor, Algal Res. 18 (2016) 352–359. doi:10.1016/j.algal.2016.06.016.

[77]   J.A. Raven, R.J. Geider, Temperature and algal growth, New Phytol. 110 (1988) 441–461. doi:10.1111/j.1469-8137.1988.tb00282.x.

[78]   S.P. Shukla, J. Kvíderová, J. Tříska, J. Elster, Chlorella mirabilis as a potential species for biomass production in low-temperature environment, Front. Microbiol. 4 (2013) 1–12. doi:10.3389/fmicb.2013.00097.

[79] W. Zillig, K. Lenz, K. Sedlbauer, M. Krus, Condensation on façades - influences of construction type and orientation, Res. Build. Phys. (2003) 437–444. https://www.irbnet.de/daten/iconda/CIB2387.pdf.

[80] M. Morelli, T.R. Nielsen, G.A. Scheffler, S. Svendsen, Internal Insulation of Masonry Walls with Wooden Floor Beams in Northern Humid Climate, Therm. Perform. Exter. Envel. Whole Build. XI Int. Conf. (2010).

[81] M. Morelli, S. Svendsen, Investigation of interior post-insulated masonry walls with wooden beam ends, J. Build. Phys. 36 (2013) 265–273. doi:10.1177/1744259112447928.

[82] E. Di Giuseppe, Nearly Zero Energy Buildings and Proliferation of Microorganisms, Springer, Cham, 2013. doi:https://doi.org/10.1007/978-3-319-02356-4.

[83] H.M. Künzel, Factors determining surface moisture on external walls, Build. X. (2007) 6.

[84] B. Chen-Charpentier, Numerical simulation of biofilm growth in porous media, J. Comput. Appl. Math. 103 (1999) 55–66. doi:10.1016/S0377-0427(98)00240-4.

[85] F. Clarelli, C. Di Russo, R. Natalini, rib, A fluid dynamics multidimensional model of biofilm growth: stability, influence of environment and sensitivity, Math. Med. Biol. (2015) 1–26. doi:10.1093/imammb/dqnxxx.

[86] F. Clarelli, C. Di Russo, R. Natalini, M. Ribot, A fluid dynamics model of the growth of phototrophic biofilms, J. Math. Biol. 66 (2013) 1387–1408. doi:10.1007/s00285-012-0538-5.

[87] F. Clarelli, C.D.I. Russo, R. Natalini, M. Ribot, Mathematical models for biofilms on the surface of monuments, Appl. Ind. Math. Italy III, 9th Conf. SIMAI. 82 (2009) 1–12.

[88] T. Thu Hien, N.-D. Hoang, Predicting Colonization Growth of Algae on Mortar Surface with Artificial Neural Network, J. Comput. Civ. Eng. Accepted, (2016).

[89] T.H. Tran, N.D. Hoang, Estimation of algal colonization growth on mortar surface using a hybridization of machine learning and metaheuristic optimization, Sadhana - Acad. Proc. Eng. Sci. 42 (2017) 929–939. doi:10.1007/s12046-017-0652-6.

[90] M. Avrami, Kinetics of Phase Change. II Transformation-Time Relations for Random Distribution of Nuclei, J. Chem. Phys. 8 (1940) 212–224. doi:10.1063/1.1750631.

[91] M. Avrami, Granulation, Phase Change, and Microstructure Kinetics of Phase

Change. III, J. Chem. Phys. 9 (1941) 177–184. doi:10.1063/1.1750872.

[92]   M. Avrami, Kinetics of phase change. I: General Theory, J. Chem. Phys. 7 (1939) 1103–1112.

[93]   W.A. Johnson, R.F. Mehl, Reaction kinetics in processes of nucleation and growth, Trans. AIME. 135 (1939) 416. doi:10.1007/s11663-010-9421-1.

[94]   M. Fanfoni, M. Tomellini, The Johnson-Mehl- Avrami-Kohnogorov model: A brief review, Nuovo Cim. D. 20 (1998) 1171–1182. doi:10.1007/BF03185527.

[95]   B. Ruot, H. Barberousse, Quantification and kinetic modelling of the colonisation of façades rendering mortars by algae, (2007).

[96]   W. Jin, S.W. McCue, M.J. Simpson, Extended logistic growth model for heterogeneous populations, J. Theor. Biol. 445 (2018) 51–61. doi:10.1016/J.JTBI.2018.02.027.

[97]   P.F. Verhulst, Recherches mathématiques sur la loi d'accroissement de la population, Nouv. Mémoires l'Académie R. Des Sci. B.-Lett. Bruxelles. 18 (1845) 14–54. http://eudml.org/doc/182533.

[98]   T. Tashiro, F. Yoshimura, A neo-logistic model for the growth of bacteria, Phys. A Stat. Mech. Its Appl. 525 (2019) 199–215. doi:10.1016/J.PHYSA.2019.03.049.

[99]   E. Lee, M. Jalalizadeh, Q. Zhang, Growth kinetic models for microalgae cultivation: A review, Algal Res. 12 (2015) 497–512. doi:10.1016/J.ALGAL.2015.10.004.

[100]   D. Surendhiran, M. Vijay, B. Sivaprakash, A. Sirajunnisa, Kinetic modeling of microalgal growth and lipid synthesis for biodiesel production, 3 Biotech. 5 (2015) 663–669. doi:10.1007/s13205-014-0264-3.

[101]   H.T. Banks, E. Collins, K. Flores, P. Pershad, M. Stemkovski, L. Stephenson, Statistical error model comparison for logistic growth of green algae (Raphidocelis subcapitata), Appl. Math. Lett. 64 (2017) 213–222. doi:10.1016/J.AML.2016.09.006.

[102]   R. Khalseh, Evaluation of different kinetics for bioethanol production with emphasis to analytical solution of substrate equation, Theor. Found. Chem. Eng. 50 (2016) 392–397. doi:10.1134/S0040579516040357.

[103]   L. Xin, H. Hong-ying, G. Ke, S. Ying-xue, Effects of different nitrogen and phosphorus concentrations on the growth, nutrient uptake, and lipid accumulation of a freshwater microalga Scenedesmus sp., Bioresour. Technol. 101 (2010) 5494–5500. doi:10.1016/j.biortech.2010.02.016.

[104] M. Stemkovski, R. Baraldi, K.B. Flores, H.T. Banks, Validation of a mathematical model for green algae (Raphidocelis subcapitata) growth and implications for a coupled dynamical system with Daphnia magna, Appl. Sci. 6 (2016). doi:10.3390/app6050155.

[105] International Energy Agency, Guidelines and Practice, Annex XIV Condens. Energy. (1990). http://www.ecbcs.org/docs/annex_14_guidelines_and_practice.pdf.

[106] N.J. Rowan, C.M. Johnstone, R.C. McLean, J.G. Anderson, J.A. Clarke, Prediction of toxigenic fungal growth in buildings by using a novel modelling system, Appl. Environ. Microbiol. 65 (1999) 4814–4821.

[107] Hannu Viitanen, A.-C. Ritschkoff, T. Ojanen, M. Salonvaara, Moisture conditions and biodeterioration risk of building materials and structure., J. Build. Phys. 1 (2002) 1–6. doi:10.1177/1744259109343511.

[108] A. Hukka, H. Viitanen, A mathematical model of mould growth on wooden material, Wood Sci. Technol. 33 (1999) 475–485. doi:10.1007/s002260050131.

[109] T. Ojanen, H. Viitanen, R. Peuhkuri, K. Lähdesmäki, J. Vinha, K. Salminen, Mold Growth Modeling of Building Structures Using Sensitivity Classes of Materials, Therm. Perform. Exter. Envel. Build. XI. (2010) 1–10. doi:10.1081/E-EEE2-120046011.

[110] L. Graziani, E. Quagliarini, A. Osimani, L. Aquilanti, F. Clementi, C. Yéprémian, V. Lariccia, S. Amoroso, M. D'Orazio, Evaluation of inhibitory effect of TiO2 nanocoatings against microalgal growth on clay brick façades under weak UV exposure conditions, Build. Environ. 64 (2013) 38–45. doi:10.1016/j.buildenv.2013.03.003.

[111] A. Viani, G. Cultrone, K. Sotiriadis, R. Ševčík, P. Šašek, The use of mineralogical indicators for the assessment of firing temperature in fired-clay bodies, Appl. Clay Sci. 163 (2018) 108–118. doi:10.1016/J.CLAY.2018.07.020.

[112] C. Coletti, G. Cultrone, L. Maritan, C. Mazzoli, Combined multi-analytical approach for study of pore system in bricks: How much porosity is there?, Mater. Charact. 121 (2016) 82–92. doi:10.1016/J.MATCHAR.2016.09.024.

[113] G. Cultrone, E. Sebastián, K. Elert, M.J. de la Torre, O. Cazalla, C. Rodriguez–Navarro, Influence of mineralogy and firing temperature on the porosity of bricks, J. Eur. Ceram. Soc. 24 (2004) 547–564. doi:10.1016/S0955-2219(03)00249-8.

[114] L. Graziani, E. Quagliarini, M. D'Orazio, Prevention of algal growth on clay façades by photocatalytic TiO2 nano- coating, (2015).

80

[115]   A. Dubosc, Etude de devellopement de salissures biologiques sur les parements en beton: mise au point d'essais acceleres de viellissement, Lab. Matériaux Durabilité Des Constr. (2000).

[116]   H. Barberousse, Etude de la diversite des algues et des cyanobacteries colonisant les revetements de facade en France et recherche des facteurs favorisant leur implantation, (2007).

[117]   ASTM D4404-10. Standard test method for determination of pore volume and pore volume distribution of soil and rock by mercury intrusion porosimetry. American Society for Testing and Materials, (2010).

[118]   UNI EN ISO 4287:2009. Geometrical Product Specifications (GPS) – Surface texture: Profile Method – Terms, Definitions and Surface Texture Parameters, International Standards Organization, (2009).

[119]   UNI EN ISO 12571:2013. Hygrothermal performance of building materials and products - Determination of hygroscopic sorption properties, (2013).

[120]   Chemical Engineers' Handbook. Second edition (Perry, John H., ed.), 1942. doi:10.1021/ed019p449.2.

[121]   F. Stazi, B. Gregorini, A. Gianangeli, G. Bernardini, E. Quagliarini, Design of a smart system for indoor climate control in historic underground built environment, Energy Procedia. 134 (2017) 518–527. doi:10.1016/J.EGYPRO.2017.09.558.

[122]   B. Gregorini, G. Bernardini, A. Gianangeli, E. Quagliarini, M. D'Orazio, A "smart" low-impact system for guaranteeing sustainable visitor's access, in: R. Amoeda, S. Lira, C. Pinheiro, J.M.S. Zaragoza, J.C. Serrano, F.G. Carrillo (Eds.), Herit. 2018 - Prcoeedings 6th Int. Confernce Herit. Sustain. Dev., Editorial Universidad de Granada, Granada, 2018: pp. 493–503.

[123]   B. Gregorini, A. Gianangeli, G. Bernardini, E. Quagliarini, M. D'Orazio, Building Heritage Cognitivo: un sistema per la gestione e la conservazione dell'edificio storico, in: F. Cuboni, G. Desogus, E. Quaquero (Eds.), Colloqui.AT.e 2018 - Edil. Circ., 1st Editio, Edicom Edizioni, Cagliari, 2018: pp. 529–539.

[124]   B. Gregorini, A. Gianangeli, G. Bernardini, M. D'Orazio, E. Quagliarini, La conservazione dell'ambiente ipogeo di Palazzo Campana: monitoraggi e prove di caratterizzazione propedeutici all'intervento, in: F. Minutoli (Ed.), REUSO 2018 - L'ntreccio Dei Saperi per Rispettare Passato Interpret. Present. Salvaguardare Futur., Gangemi Editore, 2018: pp. 529–538.

[125]   M. D'Orazio, E. Quagliarini, G. Bernardini, B. Gregorini, A. Gianangeli, Sustainable fruition as a preventive conservation strategy for hypogeum artefacts, J. Cult. Herit.

46 (2020) 235–243. doi:10.1016/j.culher.2020.07.011.

[126] B. Gregorini, M. Lucesoli, G. Bernardini, E. Quagliarini, M. D'Orazio, Combining Conservation and Visitors' Fruition for Sustainable Building Heritage Use: Application to a Hypogeum, in: Sustain. Energy Build. Proc. SEB 2019, Springer Singapore, 2020: pp. 269–279. doi:10.1007/978-981-32-9868-2.

[127] L. Graziani, E. Quagliarini, F. Bondioli, M. D'Orazio, Durability of self-cleaning TiO2 coatings on fired clay brick façades: Effects of UV exposure and wet & dry cycles, Build. Environ. 71 (2014) 193–203. doi:10.1016/j.buildenv.2013.10.005.

[128] A. Stazi, M. D'Orazio, E. Quagliarini, In-life prediction of hygrometric behaviour of buildings materials: an application of fractal geometry to the determination of adsorption and suction properties, Build. Environ. 37 (2002) 733–739. doi:10.1016/S0360-1323(01)00064-6.

[129] D.R. Tobergte, S. Curtis, Applied statistics using SSPS, Statistica, Matlab and R, Journal of Chemical Information and Modeling, 2013. doi:10.1017/CBO9781107415324.004.

[130] J.H. Stock, M.W. Watson, Introduction to Econometrics, Third Edit, Pearson, 2015. http://library1.nida.ac.th/termpaper6/sd/2554/19755.pdf.

[131] MathWorks, Curve Fitting Toolbox - User 's Guide - Matlab R2017b, 2017.